Graduate School ETD Form 9
(Revised 12/07)

PURDUE UNIVERSITY
GRADUATE SCHOOL
Thesis/Dissertation Acceptance

This is to certify that the thesis/dissertation prepared

By Debanjan Deep

Entitled
A Study of Blood Flow in Normal and Dilated Aorta

For the degree of Master of Science in Mechanical Engineering

Is approved by the final examining committee:

Whitney Yu
Chair

Likun Zhu

Tamer Wasfy

To the best of my knowledge and as understood by the student in the *Research Integrity and Copyright Disclaimer (Graduate School Form 20)*, this thesis/dissertation adheres to the provisions of Purdue University's "Policy on Integrity in Research" and the use of copyrighted material.

Approved by Major Professor(s): Whitney Yu

Approved by: Sohel Anwar 10/07/2013
Head of the Graduate Program Date

A STUDY OF BLOOD FLOW IN NORMAL AND DISEASED AORTA

A Thesis

Submitted to the Faculty

of

Purdue University

by

Debanjan Deep

In Partial Fulfillment of the

Requirements for the Degree

of

Master of Science in Mechanical Engineering

December 2013

Purdue University

Indianapolis, Indiana

The work is dedicated to my beloved family and friends

ACKNOWLEDGMENTS

First of all, I want to acknowledge the continuous guidance and immense support of my thesis supervisor, Dr.Whitney Yu to make this research possible. Also I would like to thank contribution of Dr. Shawn Teague of Radiology department, IU School of Medicine for providing me with the dicom data for the aorta models used in this work, providing necessary direction to proceed. Next, my gratitude goes to Saurabh Prabhakar of Ansys Inc. for his earnest support in FSI modeling and simulation part of the thesis. Last but not the least,I want to express my gratitude to my family and friends whose continuous support motivated me to accomplish this research.

TABLE OF CONTENTS

LIST OF FIGURES

ABSTRACT

Deep, Debanjan. M.S.M.E., Purdue University, December 2013. A Study of Blood Flow in Normal and Diseased Aorta. Major Professor: Whitney Yu.

Atherosclerotic lesions of human beings are common diagnosed in regions of arterial branching and curvature. The prevalence of atherosclerosis is usually associated with hardening and ballooning of aortic wall surfaces because of narrowing of flow path by the deposition of fatty materials, platelets and influx of plasma through intimal wall of Aorta. High Wall Shear Stress (WSS) is proved to be the main cause behind all these aortic diseases by physicians and researchers. Due to the fact that the atherosclerotic regions are associated with complex blood flow patterns, it has believed that hemodynamics and fluid-structure interaction play important roles in regulating atherogenesis. As one of the most complex flow situations found in cardiovascular system due to the strong curvature effects, irregular geometry, tapering and branching, and twisting, theoretical prediction and in vivo quantitative experimental data regarding to the complex blood flow dynamics are substantial paucity. In recent years, computational fluid dynamics (CFD) has emerged as a popular research tool to study the characteristics of aortic flow and aim to enhance the understanding of the underlying physics behind arteriosclerosis. In this research, we study the hemodynamics and flow-vessel interaction in patient specific normal (healthy) and dilated (diseased) aortas using Ansys-Fluent and Ansys-Workbench. The computation consists of three parts: segmentation of arterial geometry for the CFD simulation from computed tomography (CT) scanning data using MIMICS; finite volume simulation of hemodynamics of steady and pulsatile flow using Ansys-Fluent; an attempt to perform the Fluid Structure Simulation of the normal aorta using Ansys-Workbench. Instead of neglecting the branching or smoothing out the wall for simplification as a

lot of similar computation in literature, we use the exact aortic geometry. Segmentation from real time CT images from two patients, one young and another old to represent healthy and diseased aorta respectively, is on MIMICS. The MIMICS segmentation operation includes: first cropping the required part of aorta from CT dicom data of the whole chest, masking of the aorta from coronal, axial and saggital views of the same to extract the exact 3D geometry of the aorta. Next step was to perform surface improvement using MIMICS 3-matic module to repair for holes, noise shells and overlapping triangles to create a good quality surface of the geometry. A hexahedral volume mesh was created in T-Grid. Since T-grid cannot recognize the geometry format created by MIMICS 3-matic; the required step geometry file was created in Pro-Engineer. After the meshing operation is performed, the mesh is exported to Ansys Fluent to perform the required fluid simulation imposing adequate boundary conditions accordingly. Two types of study are performed for hemodynamics. First is a steady flow driven by specified parabolic velocity at inlet. We captured the flow feature such as skewness of velocity around the aortic arch regions and vortices pairs, which are in good agreement with open data in literature. Second is a pulsatile flow. Two pulsatile velocity profiles are imposed at the inlet of healthy and diseased aorta respectively. The pulsatile analysis was accomplished for peak systolic, mid systolic and diastolic phase of the entire cardiac cycle. During peak systole and mid-systole, high WSS was found at the aortic branch roots and arch regions and diastole resulted in flow reversals and low WSS values due to small aortic inflow. In brief, areas of sudden geometry change, i.e. the branch roots and irregular surfaces of the geometry experience more WSS. Also it was found that dilated aorta has more sporadic nature of WSS in different regions than normal aorta which displays a more uniform WSS distribution all over the aorta surface. Fluid-Structure Interaction simulation is performed on Ansys-WorkBench through the coupling of fluid dynamics and solid mechanics. Focus is on the maximum displacement and equivalent stress to find out the future failure regions for the peak velocity of the cardiac cycle.

1. INTRODUCTION

Due to the advances in computer hardware and numerical algorithms, computational fluid dynamics (CFD) has emerged to reveal underlying physics of blood flow and flow-vessel interaction (FVI) in human cardiac vasculature [1, 2]. Patient-specific computation [3-8] based on magnetic resonance imaging (MRI) [9] and advanced X-ray computed tomography (CT) [10] is of considerable interest due to the strong anatomical, functional, and hemodynamic interdependency of various cardiovascular structures. The underlying physics of hemodynamics and FVI through numerical simulation and parametric analysis plays an important role to reveal new bio-markers, which can separate benign and high risk lesions with respect to their progression and eventually lead to heart attack by quantifying the degree of flow dynamics and wall stress.

If we look closer about the facts of heart diseases we find that it is the number one cause of death for both men and women in the United States, killing more than 600,000 Americans each year, cancer and stroke round out the top three [33]. It accounts for 40% of all US deaths, more than all forms of cancer combined. The most common cause of heart disease is coronary artery disease, which is a blocked or narrowed coronary artery that supplies the heart with blood. Up to 1.5 million people in the US suffer from aortic diseases; 500,000 within this group suffer from severity of the same.

One more alarming economical fact is heart disease costs the United States $316.4 billion annually [33], where aortic diseases cost 108.5 billion alone. The research is motivated by the fact that if the areas prone to aortic diseases could be pointed out by computational fluid dynamic analysis, this would help the physician to figure out the diseases and thus fatalities could have been mitigated greatly beforehand.

1.1 Hemodynamics of Aorta

Oxygen-rich blood enters the aorta, the largest artery in the body, from the left ventricle. Blood flow crosses the aortic valve and is directed toward the aortic arch arteries and descending aorta. If anyone has artery disease, those arteries become narrow and blood cannot flow as they should. Fatty matter, calcium, proteins, and inflammatory cells build up within the arteries to form plaque of different sizes. The plaque deposits are hard on the outside and soft and mushy on the inside.

When the plaque is hard, the outer shell cracks (plaque rupture), platelets (disc-shaped particles in the blood that aid clotting) come to the area, and blood clots form around the plaque. Researchers found the potential effect of blood flow in addition to blood-tissue interaction within the aorta. In the next paragraphs below this will be explained more.

The aorta is the main trunk of a series of vessels which convey the oxygenated blood to the tissues of the body for its nutrition. It commences at the upper part of the left ventricle, where it is about 3 cm. in diameter, and after ascending for a short distance, arches backward and to the left side, over the root of the left lung; it then descends within the thorax on the left side of the vertebral column, passes into the abdominal cavity through the aortic hiatus in the diaphragm, and ends, considerably diminished in size (about 1.75 cm. in diameter), opposite the lower border of the fourth lumbar vertebra, by dividing into the right and left common iliac arteries. Hence it is described in several portions, viz., the ascending aorta, the arch of the aorta, and the descending aorta, which last is again divided into the thoracic and abdominal aorta.

A brief overview of all parts of the Aorta:

Aortic root - The root is the beginning of the aorta. Starting from the aortic valve (annulus) and becoming slightly wider in diameter, it gives rise to two coronary arteries and ends at the beginning of the ascending aorta. The two coronary arteries are responsible for carrying oxygen-rich blood to the heart muscle itself.

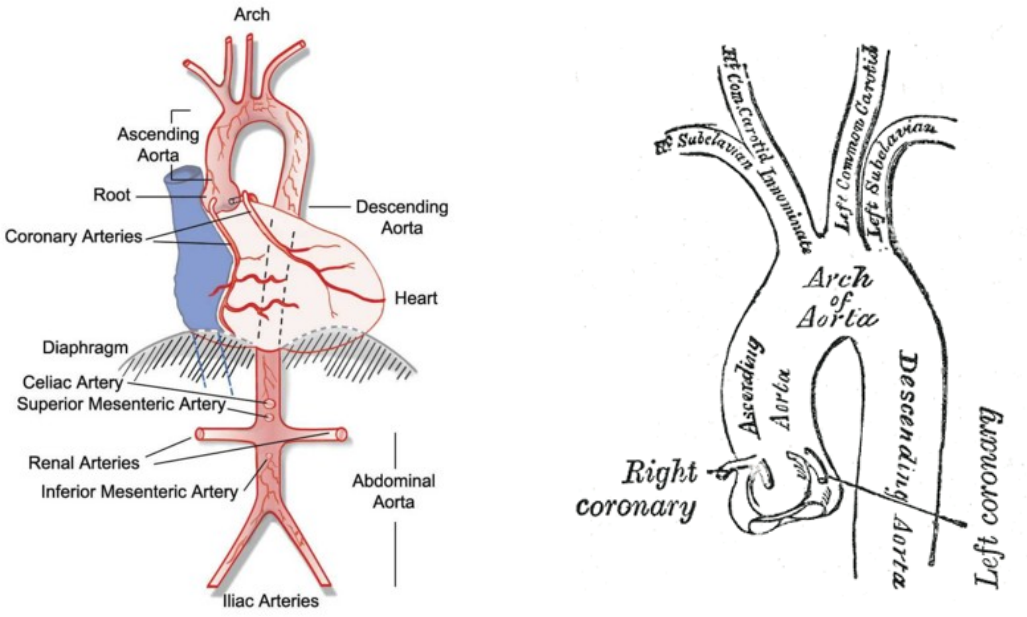

Figure 1.1. Aorta and its branches (Ref: www.cedars-sinai.edu/Patients/Programs-and-Services/Heart-Institute/)

Ascending aorta - This segment extends upward from the aortic root to the point where the innominate artery branches off the aorta, and the aorta begins to form an arch. It is within the heart sack by itself and no arteries branch from it. There is little support from surrounding tissue and it must face the entire cardiac output volume (minus the coronary arteries), making the ascending segment the most vulnerable part of the aorta.

Aortic arch - The arch represents the curved portion at the top of the aorta. The innominate, left common carotid, and left subclavian arteries, which supply blood to the head and upper body, branch from the arch. It is outside the pericardial sac and generally has better support from surrounding structures.

Descending aorta - This section begins just beyond the arch as the aorta bends down into the body. The descending aorta ends at the diaphragm. It contains the intercostal arteries that feed the spinal cord.

Thoracoabdominal aorta - This section begins at the diaphragm and ends at the visceral vessels.

Abdominal aorta - The abdominal aorta begins below the renal arteries, which supply blood to the kidneys. The aorta ends where it divides into the two iliac arteries. It contains a small artery named the inferior mesenteric artery.

1.2 Cardiovascular System Function

The cardiovascular system is one of the important organ systems of the human body that performs several vital functions. The heart is one of the most vital components of the human cardiovascular system, which is a complex organ system that performs the vital function of distributing blood throughout the body. Blood is transported to various parts of the body through a network of arteries, veins and capillaries. It is important to understand the structure of this organ system in order to comprehend how it works. The components of this body system work in tandem to facilitate the task of distribution of blood and vital nutrients throughout the body.

The heart is a hollow muscle that pumps blood throughout the blood vessels by repeated, rhythmic contractions. It is found in all animals with a circulatory system. The term cardiac (as in cardiology) means "related to the heart" and comes from the Greek , kardia, for "heart".

The vertebrate heart is principally composed of cardiac muscle and connective tissue. Cardiac muscle is an involuntary muscle tissue found only in this organ and responsible for the ability of the heart to pump blood.

The average human heart, beating at 72 beats per minute, will beat approximately 2.5 billion times during an average 66 year lifespan.

The heart has four chambers that are enclosed by thick, muscular walls. It lies between the lungs and just to the left of the middle of the chest cavity. The bottom part of the heart is divided into two chambers called the right and left ventricles,

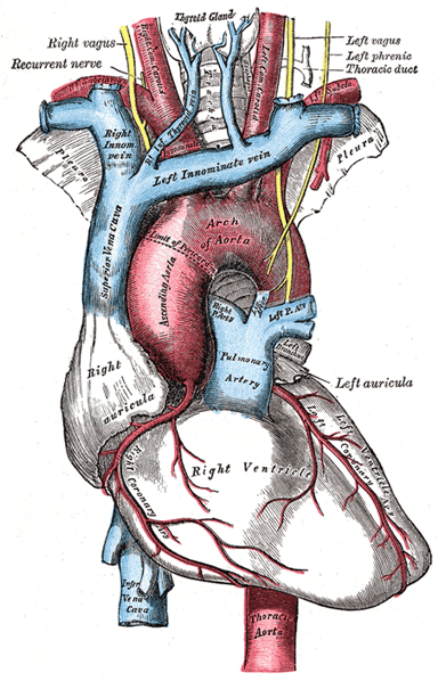

Figure 1.2. Components of Heart (Ref: www.theodora.com)

which pump blood out of the heart. A wall called the interventricular septum divides the ventricles.

The upper part of the heart is made up of the other two chambers of the heart, the right and left atria. The right and left atria receive the blood entering the heart. A wall called the interatrial septum divides the right and left atria, which are separated from the ventricles by the atrioventricular valves. The tricuspid valve separates the right atrium from the right ventricle, and the mitral valve separates the left atrium and the left ventricle.

Two other cardiac valves separate the ventricles and the large blood vessels that carry blood leaving the heart. These are the pulmonic valve, which separates the right ventricle from the pulmonary artery leading to the lungs, and the aortic valve, which separates the left ventricle from the aorta, the body's largest blood vessel.

Arteries carry blood away from the heart. They are the thickest blood vessels, with muscular walls that contract to keep the blood moving away from the heart and through the body. In the systemic circulation, oxygen-rich blood is pumped from the heart into the aorta. This huge artery curves up and back from the left ventricle, then heads down in front of the spinal column into the abdomen. Two coronary arteries branch off at the beginning of the aorta and divide into a network of smaller arteries that provide oxygen and nourishment to the muscles of the heart.

Unlike the aorta, the body's other main artery, the pulmonary artery, carries oxygen-poor blood. From the right ventricle, the pulmonary artery divides into right and left branches, on the way to the lungs where blood picks up oxygen. Aortic walls have three layers:

1. The **endothelium** is on the inside and provides a smooth lining for blood to flow over as it moves through the artery.

2. The **media** is the middle part of the artery, made up of a layer of muscle and elastic tissue.

3. The **adventitia** is the tough covering that protects the outside of the artery.

1.3 Aortic Diseases

Diseased aortic tissue is characterized by degeneration of the cells composing the aortic wall. This diseased tissue is weak, lacking sufficient elastic components to stretch and contract well. The first indication of this abnormality may be a localized enlargement in the area of weakness. When it reaches a certain size this enlarged area is referred to as an aneurysm.

Aortic tissue may also tear, even if the aorta is not enlarged. Tearing of the inner layer of the vessel wall allows blood to leak into the middle layer of the aorta, separating the inner and outer layers. This is called dissection.

1.3.1 Thoracic Aortic Aneurysms

The permanent enlargement of some portion of a blood vessel is often described as bulging, ballooning or dilation (Fig: 1.3). The diameter of the enlargement will determine whether or not it is considered an aneurysm. Traditionally for the aorta, any permanently dilated section measuring 4.0 cm or greater in diameter has been called an aneurysm.

Figure 1.3. Thoracic Aortic Aneurysm (Ref: www.sphcs.org/images)

1.3.2 Thoracic Aortic Dissection

Aortic dissection (Fig: 1.4) is the tearing of the inner layer of the aortic wall, allowing blood to leak into the wall itself and causing the separation of the inner and outer layers.

Dissection beginning in the ascending aorta is called Type A dissection. As depicted in the drawing, Type A dissection often begins just above the coronary arteries.

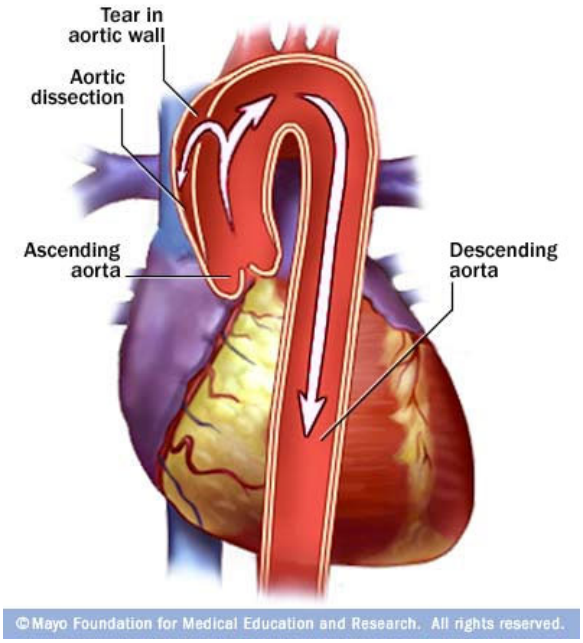

Figure 1.4. Thoracic Aortic Dissection (Ref: www.sphcs.org/images)

Dissection occurring here, where the aorta is the largest, thinnest, lacks support from surrounding structures and experiences the greatest amount of wall tension, is life threatening. Type A dissection is always treated as a surgical emergency.

1.4 Diagnosis of Aortic Diseases

Thoracic aortic disease is discovered in different ways. Sometimes there is pressure or pain in the chest or back, but most often there are no warning symptoms. A dilated aorta or aneurysm may be discovered in the course of testing for something else or perhaps as part of a routine physical. Patients may have been advised that the existence of a bicuspid aortic valve puts them at risk for aortic aneurysm or dissection. A patient may also have been told that a connective tissue disorder, such as Marfan's syndrome, is affecting the aorta and the valves of the heart.

Diagnostic testing is the first step in establishing a treatment strategy. A high degree of accuracy in the performance and interpretation of these tests is particularly critical in the evaluation of aortic disease.

1.5 Objective

The main objective to this work is to understand the hemodynamics of an aorta for a normal case and a diseased case. This was performed by comprehensive 3D finite volume simulation using Ansys for the normal and diseased aorta cases with preliminary results of FSI simulation.

The objectives of this study were achieved by realizing the following aims:

Aim 1: Image segmentation of CT Dicom data of a healthy and an aged patient to get the 3D image of their respective aortas.

Aim 2: Finite volume analysis of the aortas to compare the flow field for steady and pulsatile cases and calculate for high WSS to find out atherosclerosis prone areas.

Aim 3: Attempt to perform a very preliminary study of 2 way FSI simulation using Ansys Workbench on the normal aorta to find out the maximum deformation and equivalent stress regions of the aortic wall.

1.6 Thesis Contribution

The present work aids physicians for remedial contribution against first killer in the US (40% of all US deaths) that costs the nation approximately 385 billion dollar annually. Aortic disorder is one of the prime reasons for most of the heart diseases.

The first and foremost contribution is the computational simulation for a aorta geometry without compromising the geometry curvatures to represent actual flow modeling within a human aorta. The work also presents WSS distribution at various time phases of a cardiac cycle to determine the disease prone regions. This will be helpful for the physicians to recognize the weak regions on aortic wall to take necessary therapeutic measure beforehand.

The preliminary results of Fluid-Structure-Interaction (FSI) simulation determines the deformation and Von-Mises stress distribution while the peak flow is in progress.

2. LITERATURE REVIEW

In order to investigate the flow dynamics of the complex geometry of the human aorta, it is imperative to understand idealized flow models in simple models like curved pipes. Theoretical and experimental studies of flow in curved pipes started with the investigation of Thomson (1876) on the effect of curvature in open channels. In 1902, Williams et al. observed that the location of the maximum axial velocity is shifted toward the outer wall of a curved tube. Later, Eustice (1910) proved the presence of secondary flow by injecting ink into water flowing through a coiled pipe. The presence of secondary flows is another interesting phenomenon associated with curvature effects. Secondary flow is attributed to the physical fact that the fluid elements experience a variation in centrifugal force along their position in the arch. Dean (1927) developed analytical solutions of fully developed, steady flow in a curved tube of a circular cross section. The results explained that as the flow moves around the curved tube, an imbalance between centrifugal forces and the inwardly directed radial pressure gradient results in secondary flow developed within the tube cross section. The fluid in the core moves toward the outer wall of curvature and returns to the inner wall along the tube wall resulting in two symmetric vortices. As a result of secondary motion, the axial velocity is skewed with a maximum axial velocity magnitude found more towards the outer wall with increasing curvature (Dean, 1927 - 1928) (Fig: 2.1). Dean number: $De = 2\sqrt{(}a \times Re/R)$, where De, a, R and Re are Dean number, the pipe radius, the radius of the curvature of the pipe and Reynolds number respectively.

Aortic replacement based on computational fluid dynamics analysis has been one of the celebrated topics for last few years. In a paper, Lantz Heim et al. [11] found out the fact that high stress on residual aortic tissue may result in aneurysm formation or aneurysmal dilatation. Utilizing a computational fluid dynamic evaluation, they

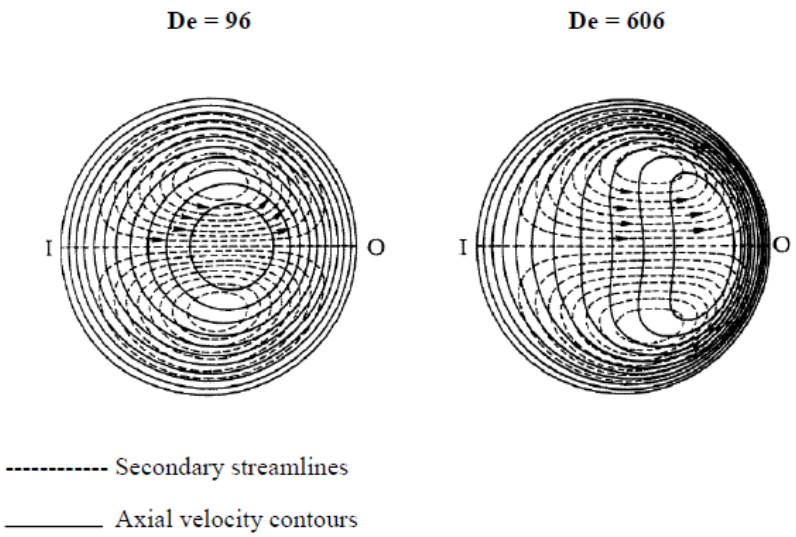

Figure 2.1. Secondary flow pattern for steady flow in curved pipe (Dean, 1927), the Effect of the Dean number on secondary flow patterns can be seen

aimed to define possible optimal operative interventions with regard to the extent of aortic replacement.

For proof of principle, a computational fluid dynamic (CFD) analysis, using Fluent 6.2 (Ansys UK Ltd, Sheffield, UK), was performed on a simplified ascending arch and descending aortic geometry. Wall shear stress in three dimensions was assessed for the standard operations: ascending aortic replacement, arch replacement and proximal descending aortic replacement. They concluded that CFD analysis of patient-specific, 3D anatomical and physiological study may direct the replacement of normal diameter aortas in the future.

In a Large Eddy Simulation (LES) of subject specific human aorta, the same authors [12] calculated the disturbed flow field and wall shear stress. It has been found that both WSS and Oscillatory Shear Index (OSI) are important with respect to formation and stability of atherosclerotic plaque (see, e.g. [13]), and that they can be used to determine the complexity of lesions [14, 15]. In this study they investigated the WSS in a subject specific human aorta using an LES turbulence model and measured

velocity profiles as boundary conditions, to increase the physiological relevance. The complex flow situation in the aorta was shown in detail and the WSS was investigated using both integrated and instantaneous values. This decomposition of WSS into pulsating and fluctuating parts increases the understanding of how WSS affects the aortic wall, and allows for both qualitative and quantitative comparisons.

Thus, the methodology described here has the potential value to identify local WSS abnormalities that might be connected to the development or progression of vascular diseases.

In their formulation, velocity profiles were measured with MRI in a plane in both the ascending and the descending aorta, and the measurement in the ascending aorta was used to provide a physiological inlet boundary condition. The Eddy-viscosity WALE model was used in their simulation and Ansys-CFX was the solver for the simulation performed there.

An industrial Bioengineering group of Department of Mechanics, Politecnico di Torino also did some research about Visualization and Quantification of Blood Flow in the Human Aorta from in vivo 4D Phase Contrast MRI to Subject-Specific Computational Hemodynamics.

They looked for some common phenomena while blood is flowing within the aorta such as helicity of flow irrespective of age and gender. Moreover they also did significant research on TAWSS (Time-averaged wall shear stress) and OSI for various inlet boundary conditions that closely matches with physiological circumstances and determined what might happen in case of varying inlet boundary situations.

For all the above simulations they used a finite volume solver, FLUENT, and Matlab to post process the data for two different Aorta models (Fig: 2.2).

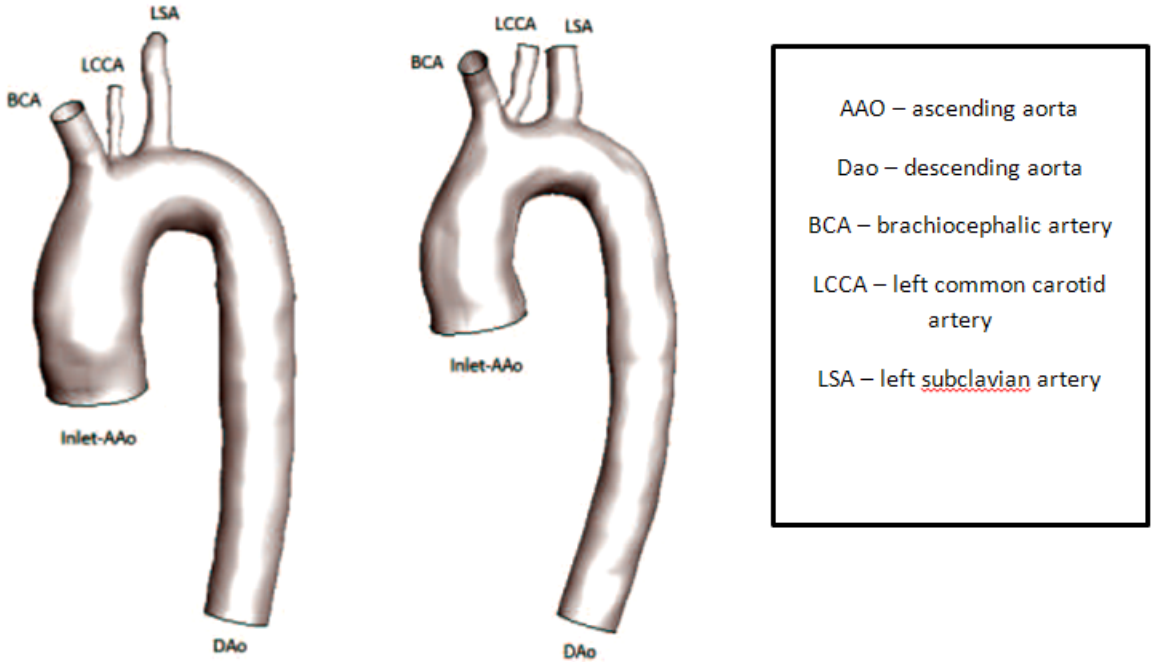

Figure 2.2. Aorta models used by the group of Politecnico di Torino [37]

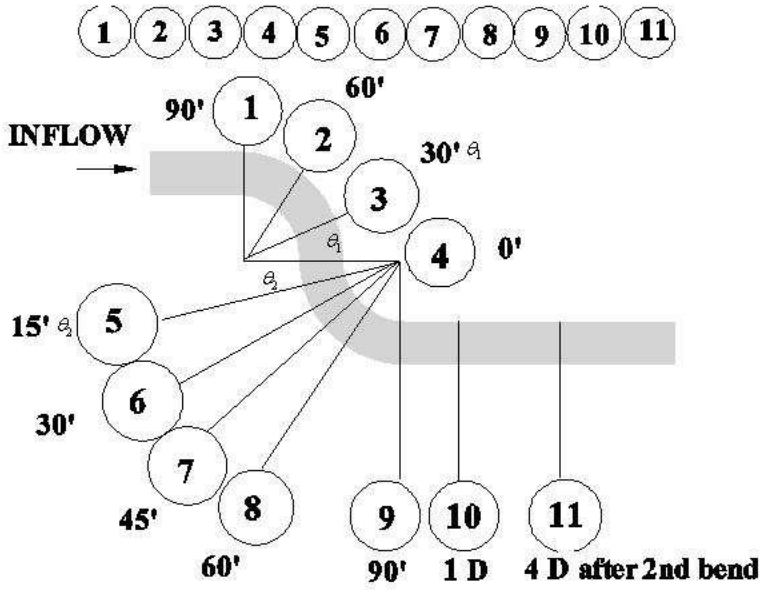

Figure 2.3. Cross sections evaluated in double bend geometries [32]

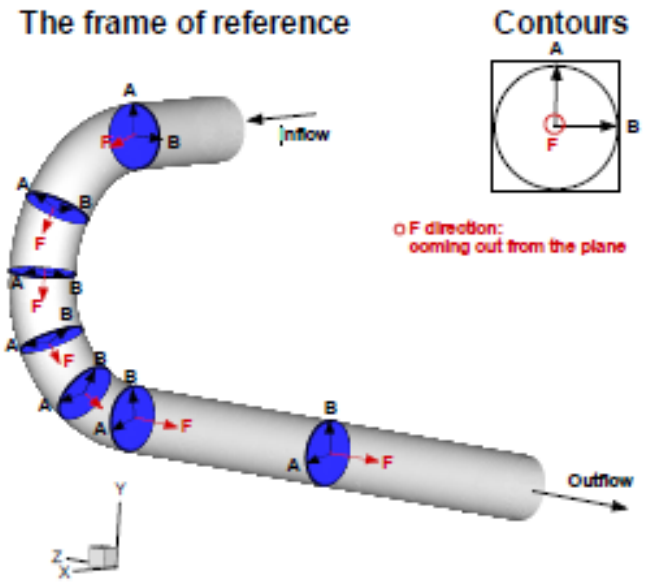

Figure 2.4. Physical orientation of each section: points A and B follow a continuous line along the geometry [32]

Moreover, in extensive research Lee and Parker [32] in their publication of spectral modeling of non-planar bends have Dean Vortex patterns within the curved flow situation. Moreover they also showed that the asymmetry of the vortices pairs reduces as Reynolds number is increasing. In the following figures (Fig: 2.4) at different cross sections they were able to demonstrate their findings.

In the publication by P.E. Vincent et al. [23] the distribution of atherosclerotic lesions within rabbit vasculature was investigated in the rabbit aortic arch and descending thoracic aorta. They were able to determine the consequences of curved flow i.e. vorticity pairs and skewness (Fig: 2.5) of velocity within the aorta as well. Moreover, they also looked for WSS distribution on the aortic wall (Fig: 2.6) for different phases of pulsatile blood flow. After that , experiments were performed on the aortic wall and they inferred that WSS is the dominant factor behind atherosclerosis and it is highly dependent on Reynolds number.

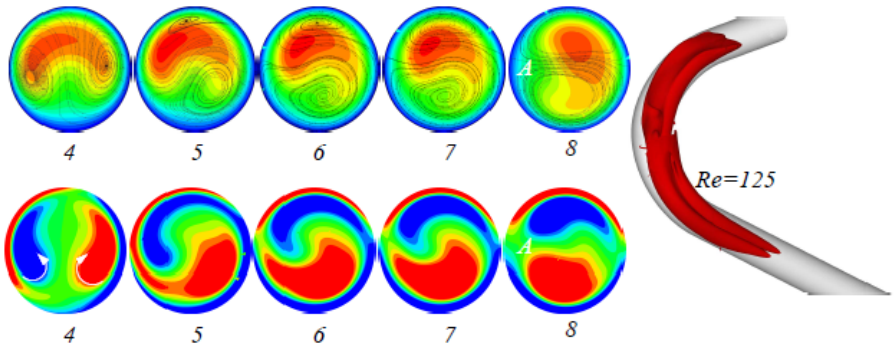

Figure 2.5. Re = 125: The isocontour shows the vortex structure highlighting the two Dean vortex patterns [32].

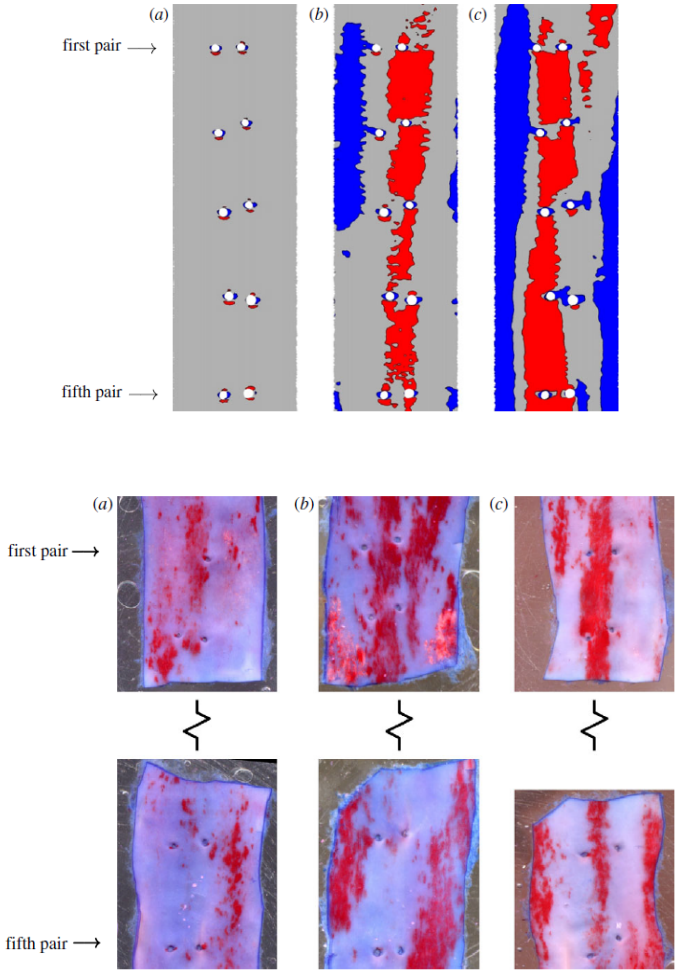

Figure 2.6. Comparison of WSS on the descending part of aorta from simulation and in vivo where from left to right Re is increasing. Blue shading denotes areas in which WSS is 75% of the average in each excised region, and red shading denotes areas in which WSS is 125% of the average in each excised region [23].

After initial studies on steady flow by Dean (1927, 1928), Womersley (1957) tackled the question of time periodicity on the laminar flow in curved and elastic pipes. Womersley used a simplified model based on linearization of the pulsatile flow in the form of a sinusoidal wave. The non-dimensional parameter (Womersley number) is defined as follows,

$\alpha = R\omega\rho/\mu$

Where R, ω , μ and ρ are vessel radius, angular frequency of the oscillation, dynamic viscosity and density, respectively. Womersley applied this linear analysis to a straight tube with a pulsatile flow in the form of a simple sinusoidal wave. The Womersley number can be considered the Reynolds number of oscillatory flows. As

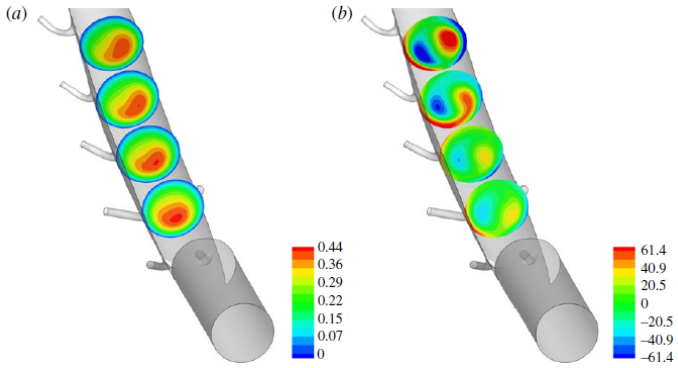

Figure 2.7. Colour maps of (a) blood velocity (ms^{-1}) and (b) vorticity (s^{-1}) perpendicular to four planes within the descending aorta in both cases, Re = 300 [23]

we move forward to dig deep into the effect of wall while the blood flow is happening within the aorta, we came across a relevant research work by F. Gao and T. Matsuzawa [16] who used a 3-layered simplified geometry of a aorta (Fig: 2.8) to investigate the Wall stress distribution and effect of medial stress on variation circumferential stress across the wall over different time period of cardiac cycle. This study lacks the force effects due to the branches but provides the first layered aorta FSI insights in accordance to carry out the dissection prone regions within Aortic Arch. The finite

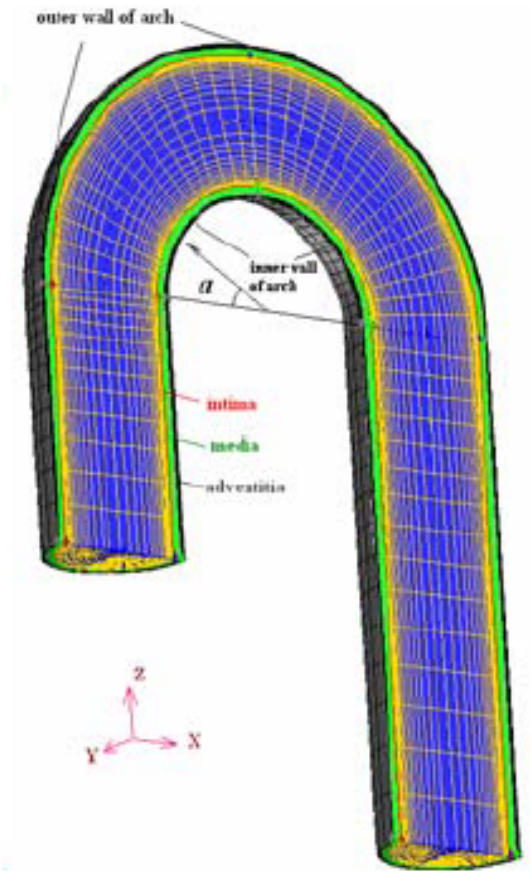

Figure 2.8. Three-layered aortic arch model. R represents the radius of the arch. The angle α represents the wall position in the median longitudinal cross-section [16]

element method (FEM) was utilized for all the computational studies reported in their work. The code Fidap (Fluent Inc., Lebanon, NH) has been used to carry out the simulation.

An exclusive study of abdominal aortic Aneurysm carried out by Florentina Ene [17] also revealed the opportunity to explore the FSI using Ansys workbench which inspired us to further our study in the arena of complex geometric aortic blood flow, which is elaborated on in Chapter 4 of this thesis.

3. CT IMAGE PROCESSING AND SEGMENTATION USING MIMICS MATERIALISE (INC.)

X-ray computed tomography, also computed tomography (CT scan), is a medical imaging procedure that uses computer-processed X-rays to produce tomographic images or 'slices' of specific areas of the body. These cross-sectional images are used for diagnostic and therapeutic purposes in various medical disciplines. Digital geometry processing is used to generate a three-dimensional image of the inside of an object from a large series of two-dimensional X-ray images taken around a single axis of rotation.

The goal of this chapter is to process the CT image slices of real patients to get the 3D images of aortas to perform blood flow simulation on them. After getting the Dicom data of a healthy and a diseased aorta from IU School of medicine, segmentation was performed to get the aortas from the CT slices using MIMICS, Materialise.

Mimics is software specially developed by Materialise for medical image processing. Mimics is used for the segmentation of 3D medical images (coming from CT, MRI, microCT, CBCT, Ultrasound, Confocal Microscopy) and the result will be highly accurate 3D models of the patients anatomy. These patient-specific models can be used for a variety of engineering applications directly in Mimics or 3-matic, or export the 3D models and anatomical landmark points to third party software, like statistical, CAD, or FEA packages.

Mimics provides a bridge from CT/MRI data to: 3D computer models, optimized surface meshes, FE and CFD analysis, physical 3D models, surgical simulation, device and implant design and traditional CAD. Mimics can import any 2D stack of images and allows transforming them into a 3D model with the utmost accuracy and flexibility in an extremely user-friendly environment. Mimics imports images like CT, TechCT, MRI and Microscopy data in a wide variety of formats, far beyond DICOM.

It is modular-based software that can be tailored to meet individual needs. The different modules can be combined into a solution that offers all the tools for powerful medical image processing and editing. Various modules will each export the file in the format needed. Some modules will also allow very specialized applications, e. g. surgical simulation. The combination of this flexibility with its powerful features and its user-friendly interface ensured that Mimics is worldwide the standard for 3D image processing.

In short Mimics is used to:

Easily and quickly create accurate 3D models from imaging data Accurately measure in 2D and 3D

Export 3D models in STL format for additive manufacturing

Export 3D models to 3-matic to optimize the mesh for FEA or CFD

3.1 Segmentation Steps

The Steps to get the 3D image from the Dicom data are as follows.

3.1.1 Cropping the Dicom Data

Cropping the required portion of the Dicom data is the first and foremost task to do for image segmentation. Since Dicom data comes with the entire chest CT scan and we just need the portion of aorta, the unnecessary portion is chopped off. The CT slice, after being chopped off looks like (Fig: 3.1):

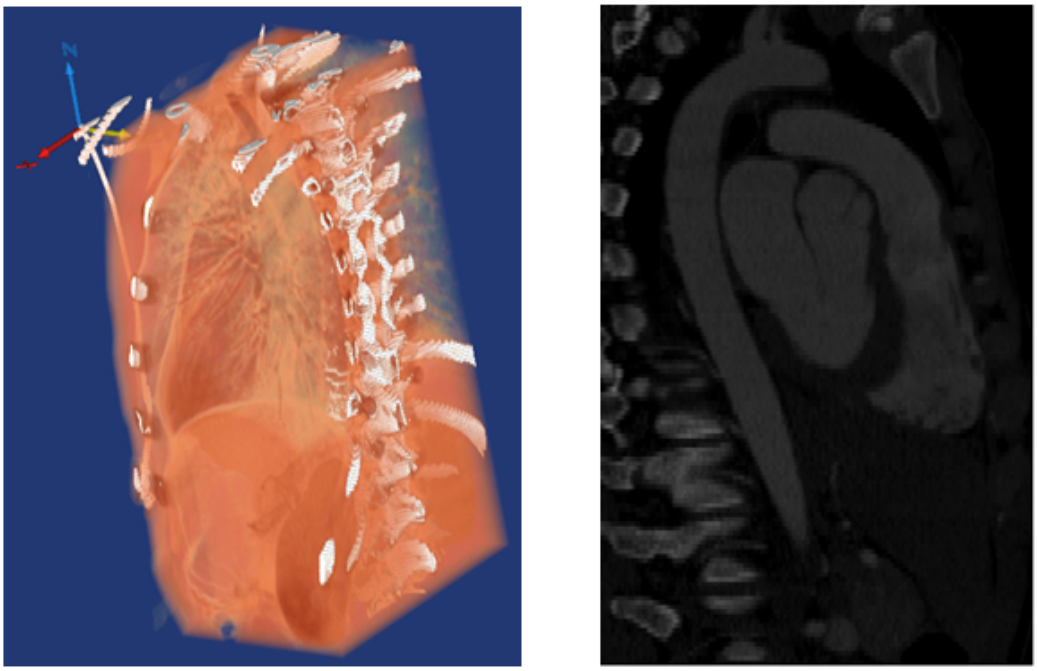

Figure 3.1. Dicom data and CT image slice (Dicom data courtesy: Radiology Department, IU School of Medicine)

3.1.2 3D Rendering and Extraction of Organs Part by Part

The 2D image slices of coronal, axial and saggital views are masked properly to extract the required part out of the Dicom data. Most of the times the segmented parts come with other organs which are required to be chopped off later, one after one, to get the desired part. In the case of diseased aorta, the tricuspid valve inlet was modified in an inclined opening to provide a more realistic BC at the inlet.

3.2 Dilation Effect of a Diseased Aorta

Since image segmentation was the tool to discover the dilation effect of the aorta, we take the privilege to illustrate our findings about dilated aorta here. Since dilation is well described in the introductory chapter of the thesis, here we discuss in brief the

reasons behind it. Dilation, also known as Aortic Aneurysm, generally happens for the following reasons:

Having a bicuspid valve instead of a normal tricuspid one.

Individuals with high blood pressure are also prime candidates for an enlarged aorta.

Tissue connectivity disorders, atherosclerosis, inflammatory conditions, Marfan syndrome and Ehlers-Danlos syndrome.

Diagnostic tools are designed to check for an enlarged aorta included in computed tomography (CT) scans and magnetic resonance imaging (MRI). Fig: 3.5 describes the Aortic dilation a bit more.

In a clinical research paper [18] the authors have provided a useful chart (Fig: 3.6) to distinguish the dilated aorta from the normal one. They also discovered that the median aortic diameter at the time of rupture for the ascending aortic arch is 6.0 cm.

Now, if we look into our dilated aorta model that we have extracted from the CT imaging technique, we could easily distinguish and infer that our model, that we extracted from the 95 year old person Fig: 3.8 , was necessarily dilated having a mean inlet diameter of about 5.58cm by comparing the above chart.

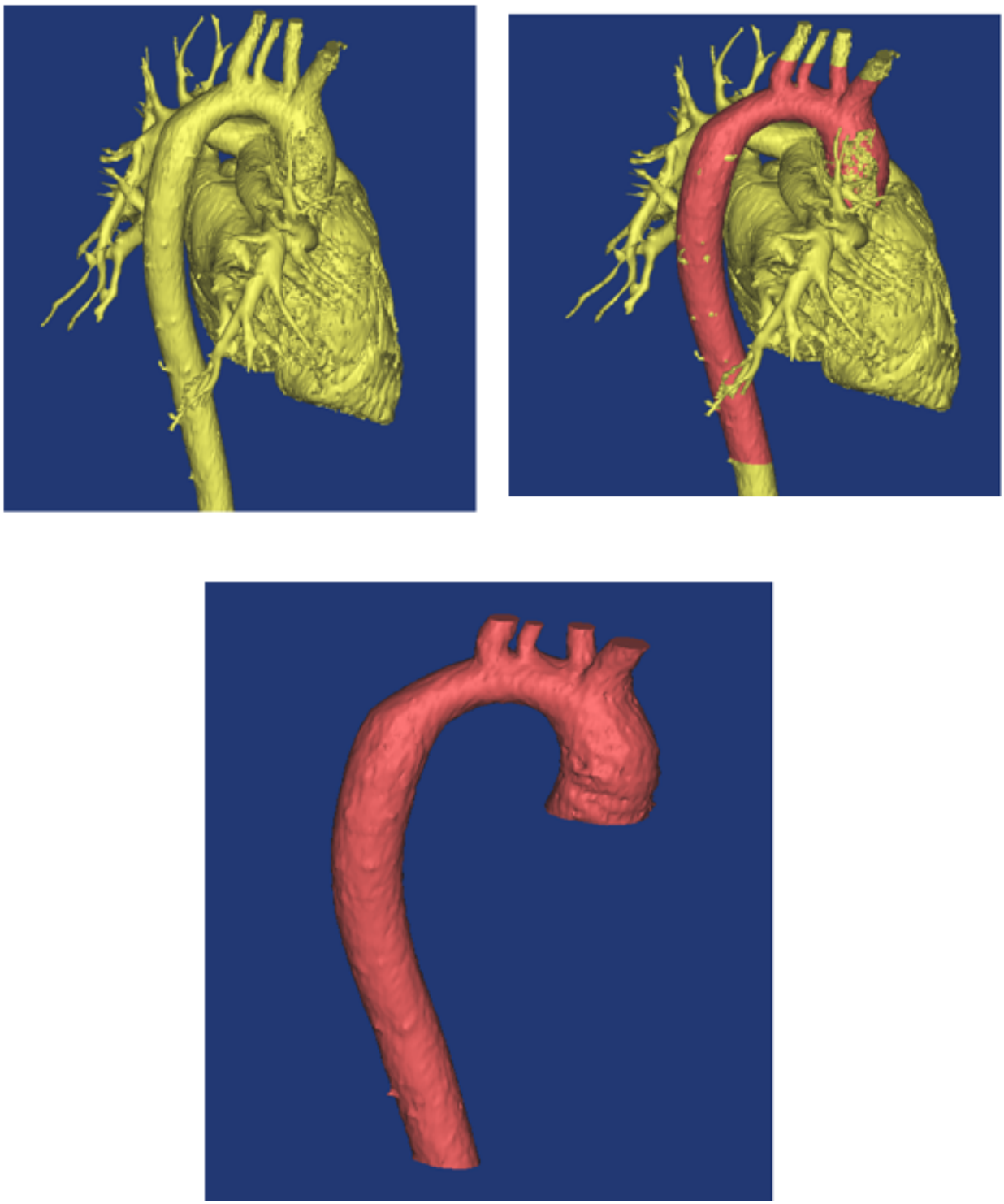

Figure 3.2. Aorta with heart (top left), Aorta masked and ready to be chopped out from (top right) and Aorta chopped out (below) (Dicom data courtesy: Radiology Department, IU School of Medicine)

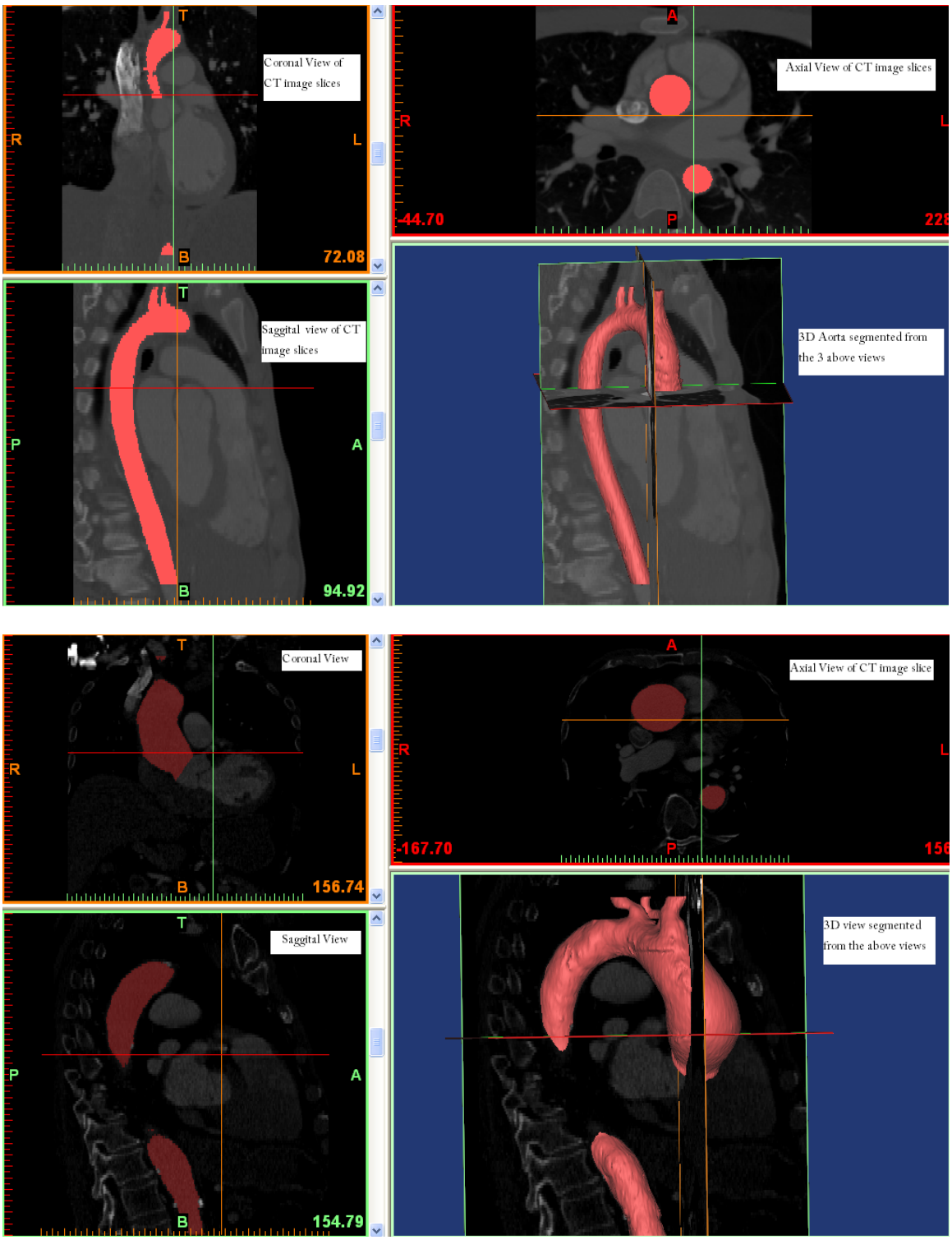

Figure 3.3. Views of normal Aorta segmentation (top) and diseased (bottom)

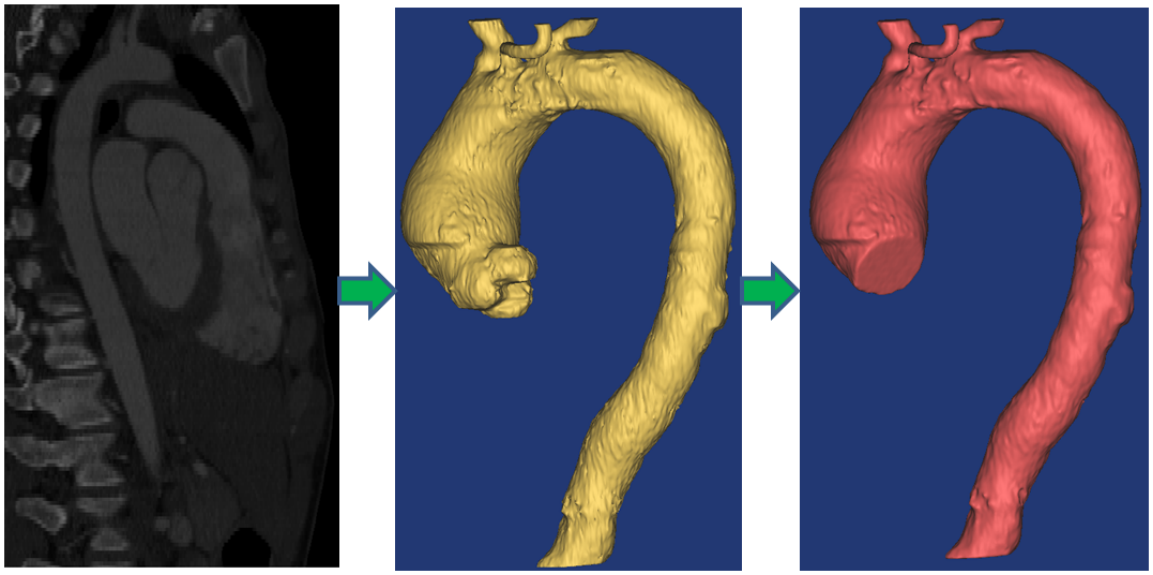

Figure 3.4. Evolution of Diseased aorta from CT dicom data

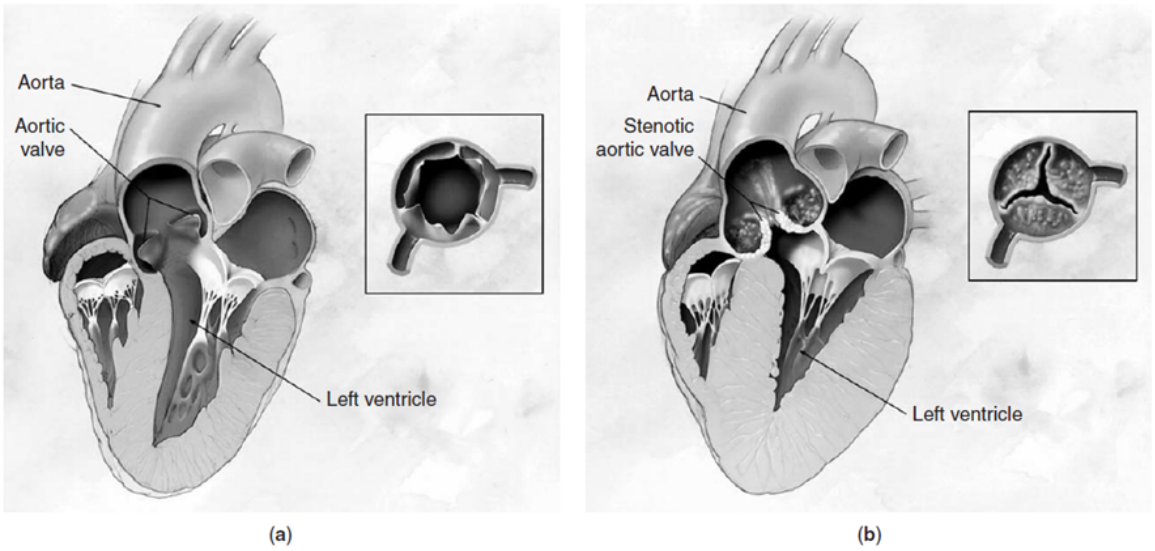

Figure 3.5. Schema of the heart during ejection. (a) Without aortic stenosis, the aortic valve is fully opened; (b) in the presence of aortic stenosis, the calcified aortic valve cannot open fully, which causes an obstruction to blood flow from the left ventricle to the aorta and produces a transvalvular flow jet [8]

Table 1. Normal Ascending Aortic Dimensions in Adults

Diameter	Value	Study
Aortic annulus, cm		
Men	2.6±0.3	TTE
Women	2.3±0.2	TTE
Sinus of Valsalva, cm		
Men	3.4±0.3	TTE
Women	3.0±0.3	TTE
Aortic root	<3.7	TTE
Proximal ascending aorta, cm		
Men	2.9±0.3	TTE
Women	2.6±0.3	TTE
Ascending aorta, cm/m^2	1.4–2.1 cm/m^2	TEE
cm	<3.8 (2.5–3.8)	CT
cm	<3.7	TTE

Reprinted with permission (modified) from Erbel et al[2] for the ESC task force. Note that computed tomography or magnetic resonance measures the external diameter and is expected to be 0.2 to 0.4 cm larger than the TTE/transesophageal echocardiography (TEE) internal diameter.[3] For younger patients, we refer to the nomograms of normal values with SDs related to body surface area in the same article.[2]

Figure 3.6. Identification of normal aorta based on diameter size [18]

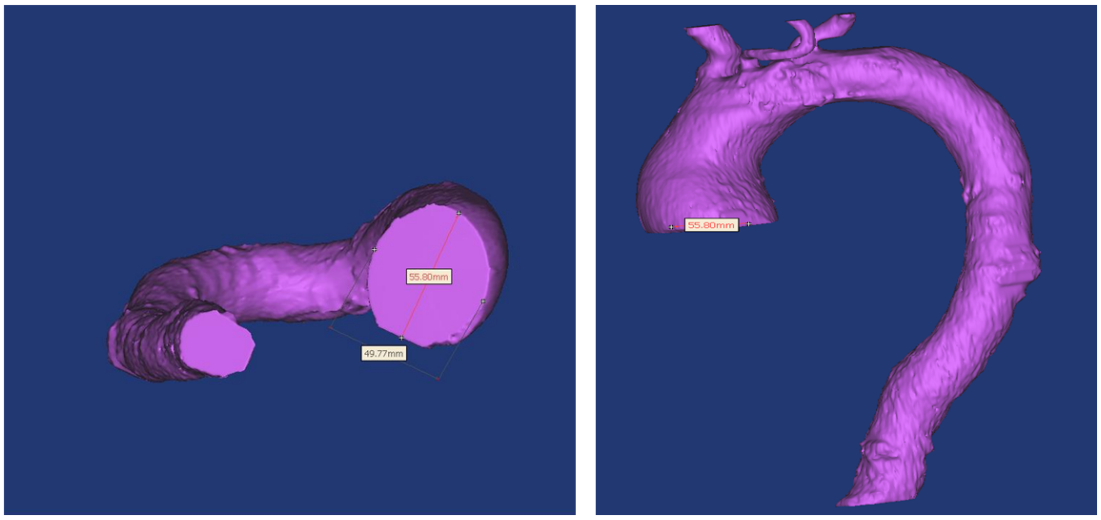

Figure 3.7. Dilated aorta dimension (Dicom data courtesy: Radiology Department, IU School of Medicine)

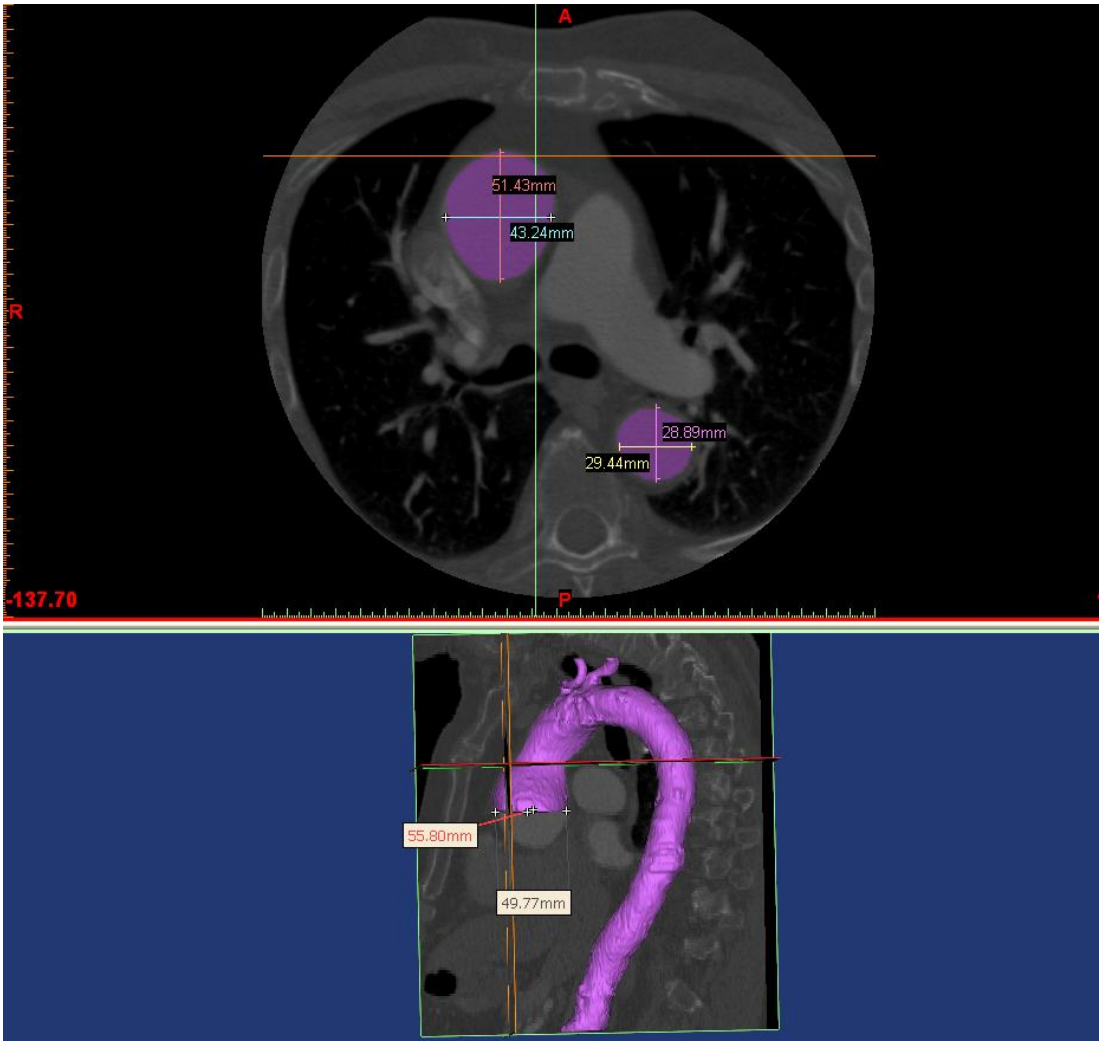

Figure 3.8. Dilated aorta dimension (Dicom data courtesy: Radiology Department, IU School of Medicine)

4. FINITE VOLUME METHOD ANALYSIS ON A NORMAL AND A DISEASED AORTA USING ANSYS FLUENT

The finite-volume method is a method for representing and evaluating partial differential equations in the form of algebraic equations [LeVeque, 2002; Toro, 1999]. Similar to the finite difference method or finite element method, values are calculated at discrete places on a meshed geometry. "Finite volume" refers to the small volume surrounding each node point on a mesh. In the finite volume method, volume integrals in a partial differential equation that contain a divergence term are converted to surface integrals, using the divergence theorem. These terms are then evaluated as fluxes at the surfaces of each finite volume. Because the flux entering a given volume is identical to that leaving the adjacent volume, these methods are conservative.

The fundamental two steps of this FVM approach is as follows:

Step 1: To divide the domain into a number of control volumes (aka cells, elements) where the variable of interest is located at the centroid of the control volume.

Step 2: Integrate the differential form of the governing equations (very similar to the control volume approach) over each control volume.

Step 3: Interpolation profiles are then assumed in order to describe the variation of the concerned variable between cell centroids. The resulting equation is called the discretized or discretization equation.

Another advantage of the finite volume method is that it is easily formulated to allow for unstructured meshes. Finite volume methods are especially powerful on coarse nonuniform grids and in calculations where the mesh moves to track interfaces or shocks. Hyman et al. (1992) [22] have derived local, accurate, reliable, and efficient finite volume methods that mimic symmetry, conservation, stability, and the duality relationships between the gradient, curl, and divergence operators on nonuniform

rectangular and cuboid grids. The method is used in many computational fluid dynamics packages.

In this thesis, a popular Finite Volume Method package named Ansys-Fluent was used to calculate flow variables and different phenomena within normal and diseased Aorta.

4.1 Governing Equations

From the mass conservation equation we know (Ref: From lecture notes of Dr. Tamer Wasfy),

$$\frac{\partial \rho}{\partial t} + \rho \frac{\partial v_i}{\partial x_i} = 0$$

where ρ is the density of the fluid, v_i is the velocity component and t is the time. Again from the momentum conservation equation we can also write,

$$\rho \frac{\partial v_i}{\partial t} = -\rho v_j \frac{\partial v_i}{\partial x_j} + \frac{\partial \sigma_{ji}}{\partial x_j} + \rho b_i$$

Where σ_{ij} is the stress in fluid can be divided into a hydtrostatic stress and a viscous stress($\sigma_{ij} = -P\delta_{ij} + \tau_{ij}$) and b_i is the body force term.

For turbulence kinetic model we have used $k - \epsilon$ model which uses two transport equations to represent the turbulent properties of the flow. The first transported variable is turbulent kinetic energy, k, which can be expressed by the following equation (Ref: $http://www.cfd-online.com/Wiki/Standardk-epsilonmodel$):

$$\frac{\partial(\rho k)}{\partial t} + \frac{\partial(\rho k v_i)}{\partial x_i} = \frac{\partial}{\partial x_j}[(\mu + \frac{\mu_t}{\sigma_k})\frac{\partial k}{\partial x_j}] + C_{1\epsilon}\frac{\epsilon}{k} + P_k - \rho\epsilon$$

where where μ_t is turbulent viscosity and S is the modulus of the mean rate of strain tensor.

$$\mu_t = \rho C_\mu \frac{k^2}{\epsilon}$$

$$P_k = \mu_t S^2$$

where S is the modulus of the mean rate of strain tensor, defined as:

$$S = \sqrt{2S_{ij}S_{ij}}$$

for dissipation ϵ,

$$\frac{\partial(\rho\epsilon)}{\partial t} + \frac{(\partial\epsilon k v_i)}{\partial x_i} = \frac{\partial}{\partial x_j}[(\mu + \frac{\mu_t}{\sigma_\epsilon})\frac{\partial\epsilon}{\partial x_j}] + C_{1\epsilon}\frac{\epsilon}{k}(P_k) - C_{2\epsilon}\rho\frac{\epsilon^2}{k} + S_\epsilon$$

Following are the values of model constants:

$C_{1\epsilon} = 1.44, C_{2\epsilon} = 1.92, C_{3\epsilon} = -0.33, C_\mu = 0.09, \sigma_k = 1.0, \sigma_\epsilon = 1.3$

4.2 Flow Simulation within the Aortas

One of the primary reasons for numerically simulating the flow in the aortic system is to understand the development of atherosclerosis and its dependence on flow structure. It has been observed that early atherosclerotic lesions develop preferentially in the vicinity of arterial branching and curvature where blood flow patterns are complex and multi-directional. The prevalence of atherosclerosis varies within the mammalian vasculature, particularly in regions of arterial branching and curvature. Since these regions are associated with complex blood flow patterns, it has been postulated that blood flow may play an important role in regulating atherogenesis. Fry [14] inferred from studies of hypercholesterolaemic animals that lesions develop in regions of high wall shear stress (WSS), hypothesizing that high WSS damaged the arterial endothelium, and hence increased lipoprotein influx into the intima.

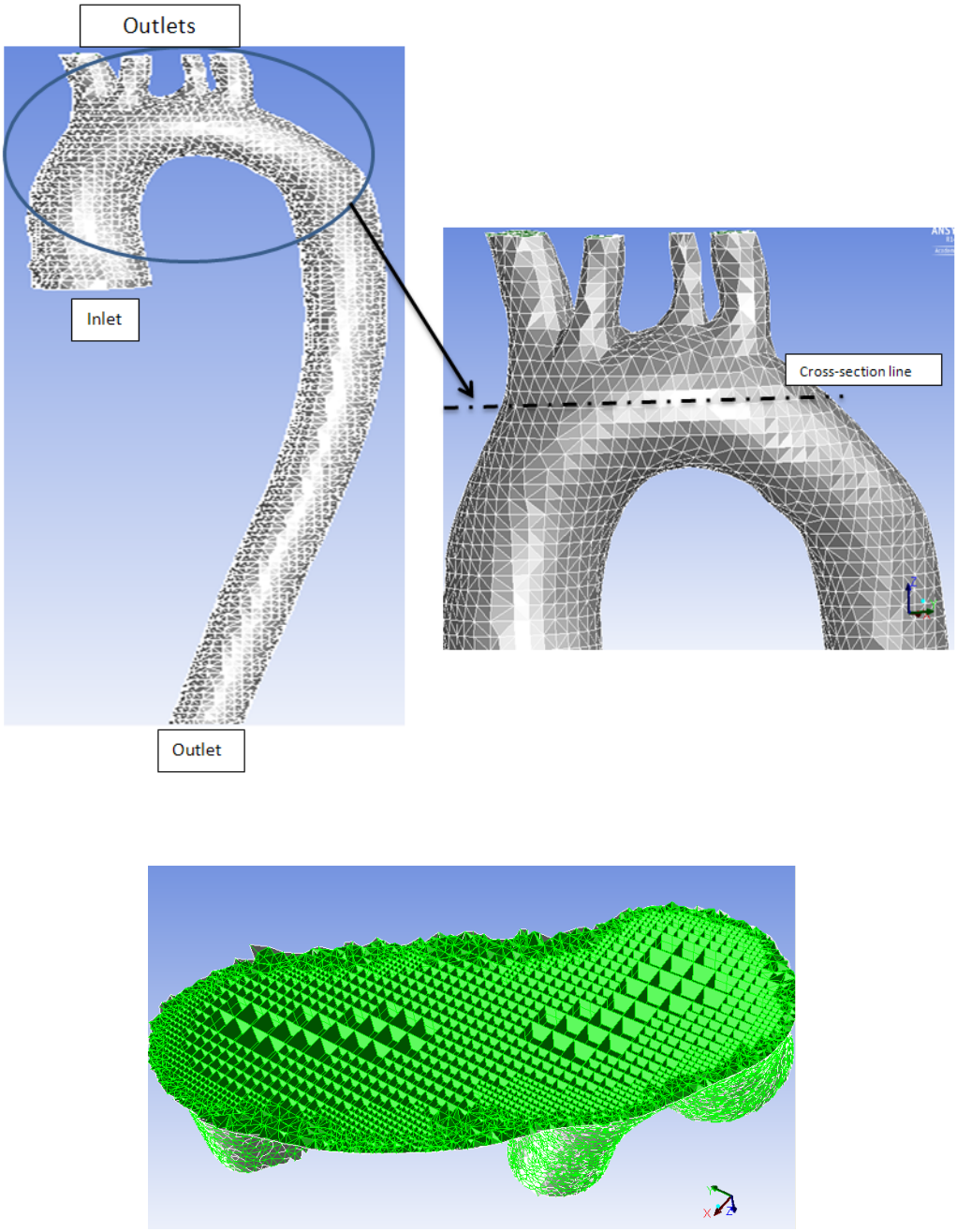

Figure 4.1. Hexahedral fluid mesh with triangular mesh on the wall of normal aorta using Tgrid.Left: the entire aorta, Right: Zoomed in view of the aortic arch, Down: Mesh examination along the cross section line. (Courtesy: Tgrid)

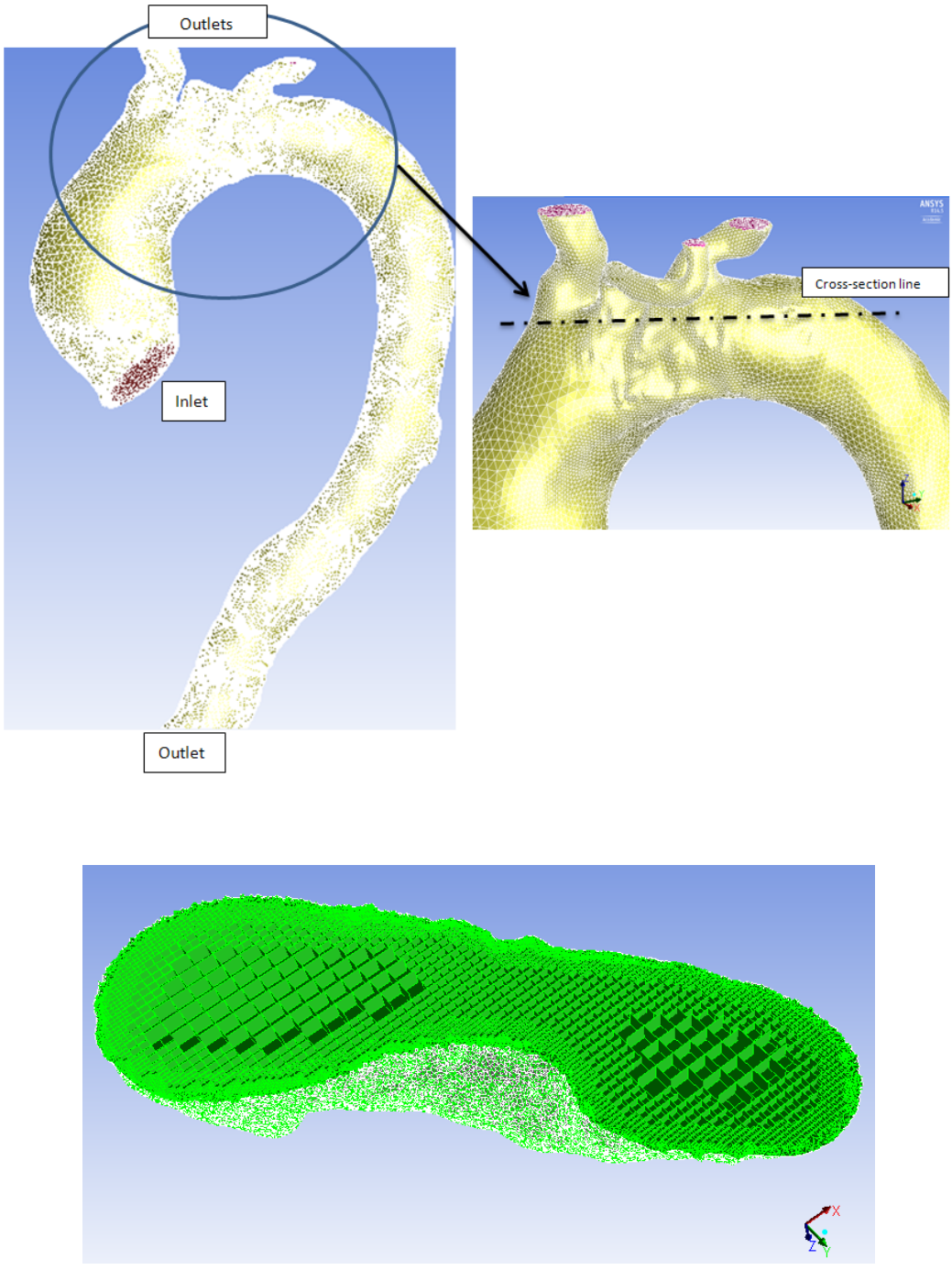

Figure 4.2. Hexahedral fluid mesh with triangular mesh on the wall of dilated aorta using Tgrid.Left: the entire aorta, Right: Zoomed in view of the aortic arch, Down: Mesh examination along the cross section line. (Courtesy: Tgrid)

Meshing was done in T-Grid (Fig: 4.1,4.2) with hexahedral mesh interior and tetrahedral transformation along the boundary. The total number of cells was around 1.8M for the normal and 3.2M for the dilated aorta.

In the present study, a Finite Volume method using Ansys-Fluent was carried out to model blood flow within a realistic representation of the human aortic arch and descending thoracic aorta for two different cases: one is a normal aorta of an 18 year old boy and the other was of a diseased aorta of a 95 year old man. The geometries was obtained from high-resolution computed tomography (CT) of a vascular cast. It included all the blood-carrying branches at the aortic arch named left common carotid artery, left subclavian artery and brachiocephalic trunk (Fig: 4.3). Interestingly enough, the normal aorta had its right subclavian artery and right common carotid artery started from the base of the aorta instead of branching out from the brachiocephalic trunk which at our knowledge has not been computationally simulated beforehand.

Three-dimensional, steady-state and pulsatile flows in the displayed aorta geometries are analyzed by solving incompressible continuity and NavierStokes equations. The analysis in this chapter did not include the distensibility of the aortic walls. In the paper [21] it was shown that the omission of the wall distensibility does not lead to a substantial deterioration for the velocity and shear stress profiles predicted for the cardiac artery. Thus the aortic walls were considered rigid for the present study.

The non-Newtonian behavior is a further challenge, which is typical for the blood flow. This is also neglected, and a fully Newtonian behavior for the blood is assumed, since it is argued [22] that departures from the Newtonian behavior start to play a role for rather small arteries, whereas we are interested in the flow in the large arteries. We also chopped off the top outlet branches of the aortas as they extend out toward the other parts of the body, to further simplify the geometry. These simplifying assumptions, such as the assumption of rigid walls and a Newtonian behavior, are common to much of the previous work in the field, including the recent ones [21, 28].

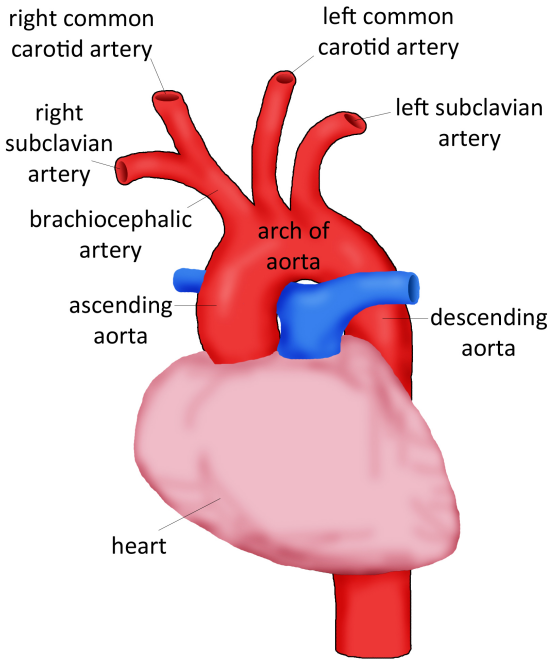

Figure 4.3. Demonstration of Aortic branches (Ref: www.chw.org/display)

Boundary Conditions: Parabolic shaped velocity was used as the boundary condition at the inlet while flow split or outflow boundary conditions were applied to represent fully developed BC. Pressure were kept constant at the outlets because the pressure data varies from different persons and the specific data was not available for the patients we studied for. Aortic wall was considered as no-slip. As initial condition, inlet velocity was used at the inlet. For pressure velocity coupling, we used PISO algorithm for both steady and pulsatile flow simulation because it improves the efficiency of the calculation performing neighbor correction and skewness correction.

In the present study, for the material properties of the blood, the following constant values are used: density: 1060 kg/m^3, dynamic molecular viscosity: 0.0035 $kg/(ms)$. The volume mesh was created in T-grid for representing the fluid part was created in T-grid ; steady and pulsatile flow simulation was performed in Ansys-Fluent and post-processing was executed in Tecplot.

4.3 Steady Flow Simulation in a Healthy and a Dilated Aorta

The main purpose of steady state simulation was to validate the simulation results with the work of E. Claes et al [29] where the authors have used a high-order-continuous Galerkin Finite Element Method to simulate blood flow within a realistic representation of the rabbit aortic arch and descending thoracic aorta. In their paper, it was also observed that two Dean-type vortices form in the aortic arch and propagate downstream the descending thoracic aorta (along with an associated skewed axial velocity profile). This leads to the occurrence of axial streaks in WSS, similar in nature to the axial streaks of lipid deposition found in the descending aorta of cholesterol-fed rabbits. Also the authors proposed various reasons why steady-state simulations were performed, as opposed to fully time-dependent studies. Primarily, the results of steady-state simulations can be analyzed with relative ease; giving insight that will facilitate interpretation of future (more complex) unsteady results, and focus on the remittance of future (more costly) unsteady studies. Also they mentioned that some disadvantages, like not being able to capture the truly unsteady flow phenomena, which is elaborately discussed already in our literature review chapter, might occur.

The steady flow analysis was performed to capture the general features of blood flow through the aorta. Hence, we chose a Reynolds number of 300 (inlet velocity for normal aorta = 0.04m/s and similarly calculated for the dilated one) at inlet to match with a previously published work. Hence the use of laminar flow as viscous flow model is justified in this simulation.

Streamlines of velocity of both a normal and a dilated aorta are demonstrated in (Fig: 4.4, 4.5).Walls are omitted in the right figures to display the streamlines better.

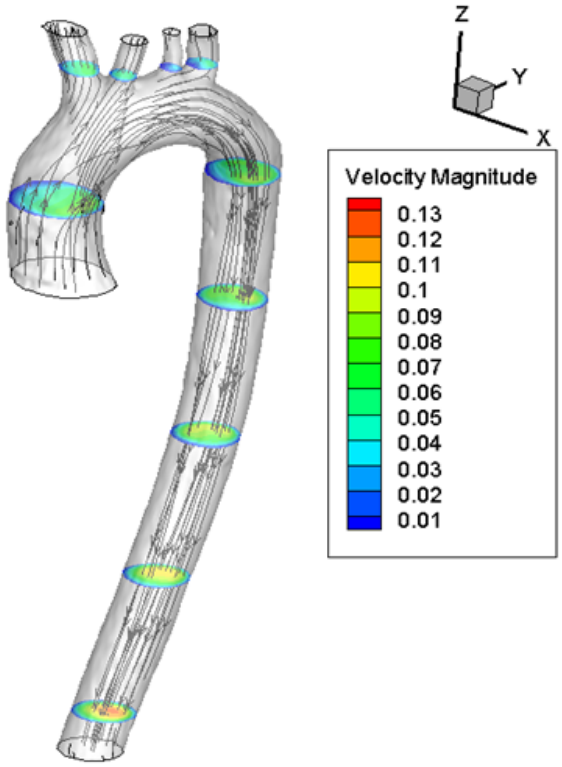

Figure 4.4. Velocity (m/s) streamlines of the normal aorta.

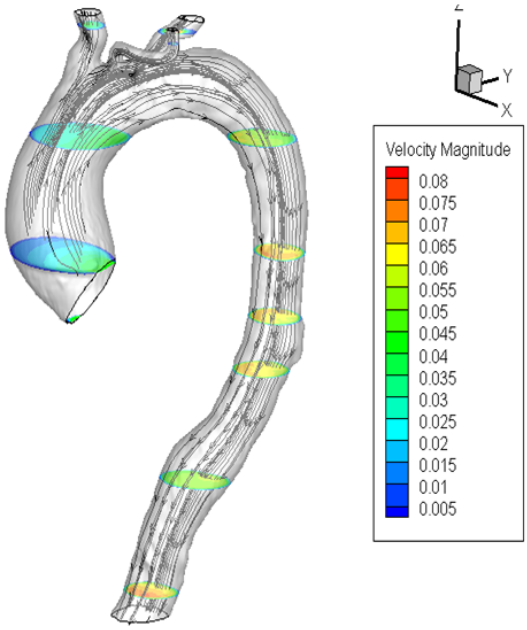

Figure 4.5. Velocity (m/s) streamlines of the dilated aorta.

We confirmed from Fig: 2.5 and 2.7 that the results of the authors [29] about the pair of vortices and velocity skewness match with our simulation results as well. To match with their computational setup, Reynolds number of 300 was taken at the inlet (inlet velocity for normal aorta = $0.04m/s$ and similarly calculated for the dilated one).

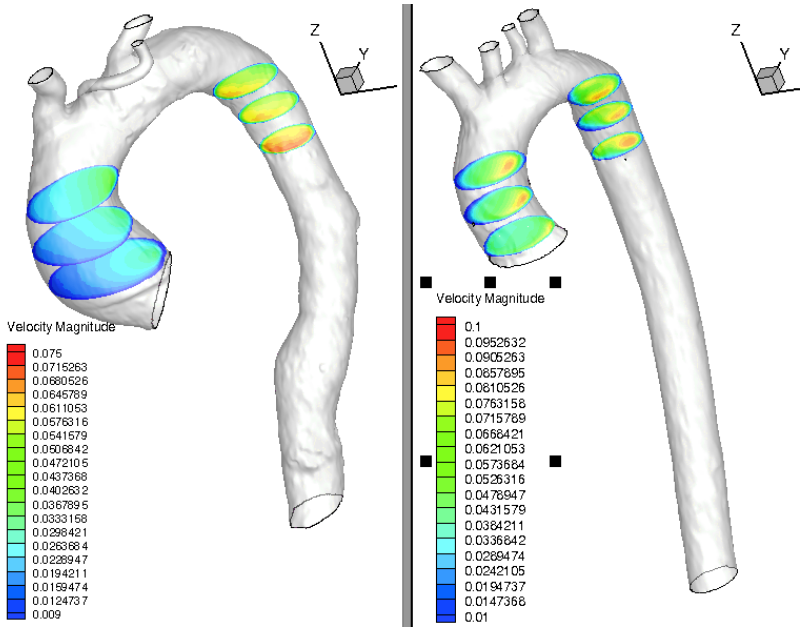

Figure 4.6. Skewed velocity profile m/s for Dilated (left) and normal(right) Aorta

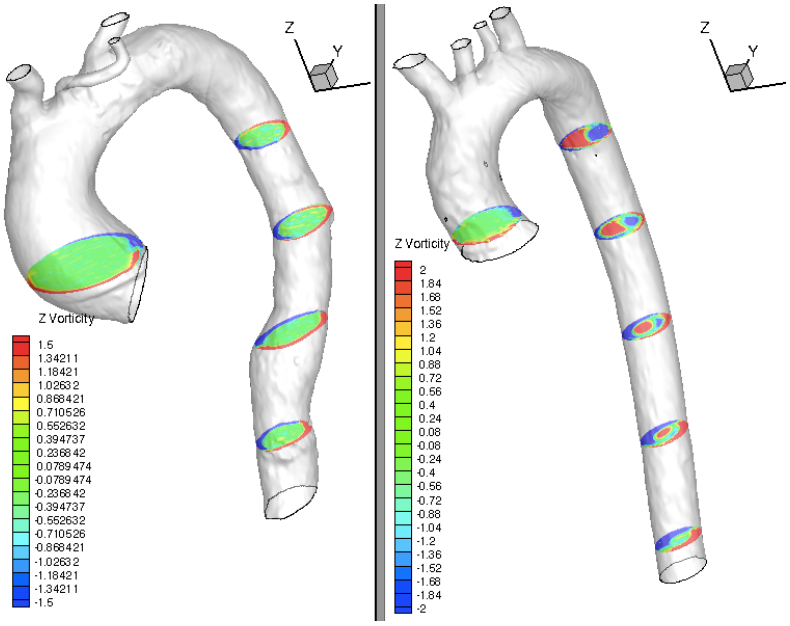

Figure 4.7. Z vorticity (s^{-1}) pairs of Dilated(left) and normal (right)

From Fig: 4.6, we can easily distinguish the skewed velocity profile towards the inner curvature of the aorta at the ascending part and outer curvature of the descending part of the aorta. Moreover from Fig: 4.7, distinct pairs of vortices were found near the aortic arch region and descending aorta part. The pairs were of similar pattern to the ones found in the aforementioned study of the authors. Thus we could come to a point of validation that our CFD code and setup has a good match with the simulation performed by the authors mentioned, and we could further proceed to investigate the WSS results, which is our primary target, to determine atherosclerosis prone regions.

4.4 Pulsatile Flow Simulation Analysis

We move forward to analyze the pulsatile flow consequences for a normal and a dilated aorta. The goal of this part is to identify the regions of future probable atherosclerosis. Thus dissection or aortic disorder could be easily identified from the

WSS analysis. It is well established in the papers [27, 28] that as the size of the inlet increases, the velocity, pressure and WSS all increase in the ascending aorta. Since the size of the inlet is directly related to the effect of dilation of the aorta, the disordered or future disordered parts could be easily identified.

Boundary Conditions: The boundary condition was same as the steady flow simulation case but the inlet velocity was of pulsatile form that is described later in this Chapter.

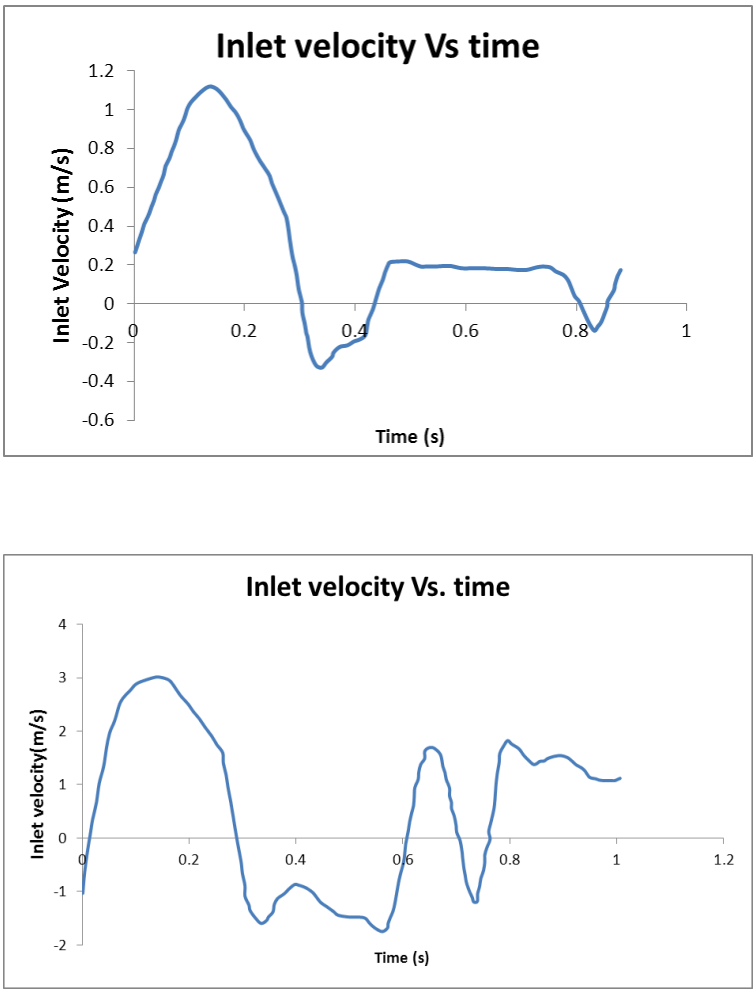

Figure 4.8. Aorta inlet velocity profile- Normal (top) and Diseased (bottom) (Courtesy- Department of Radiology, IU School of Medicine, IUPUI)

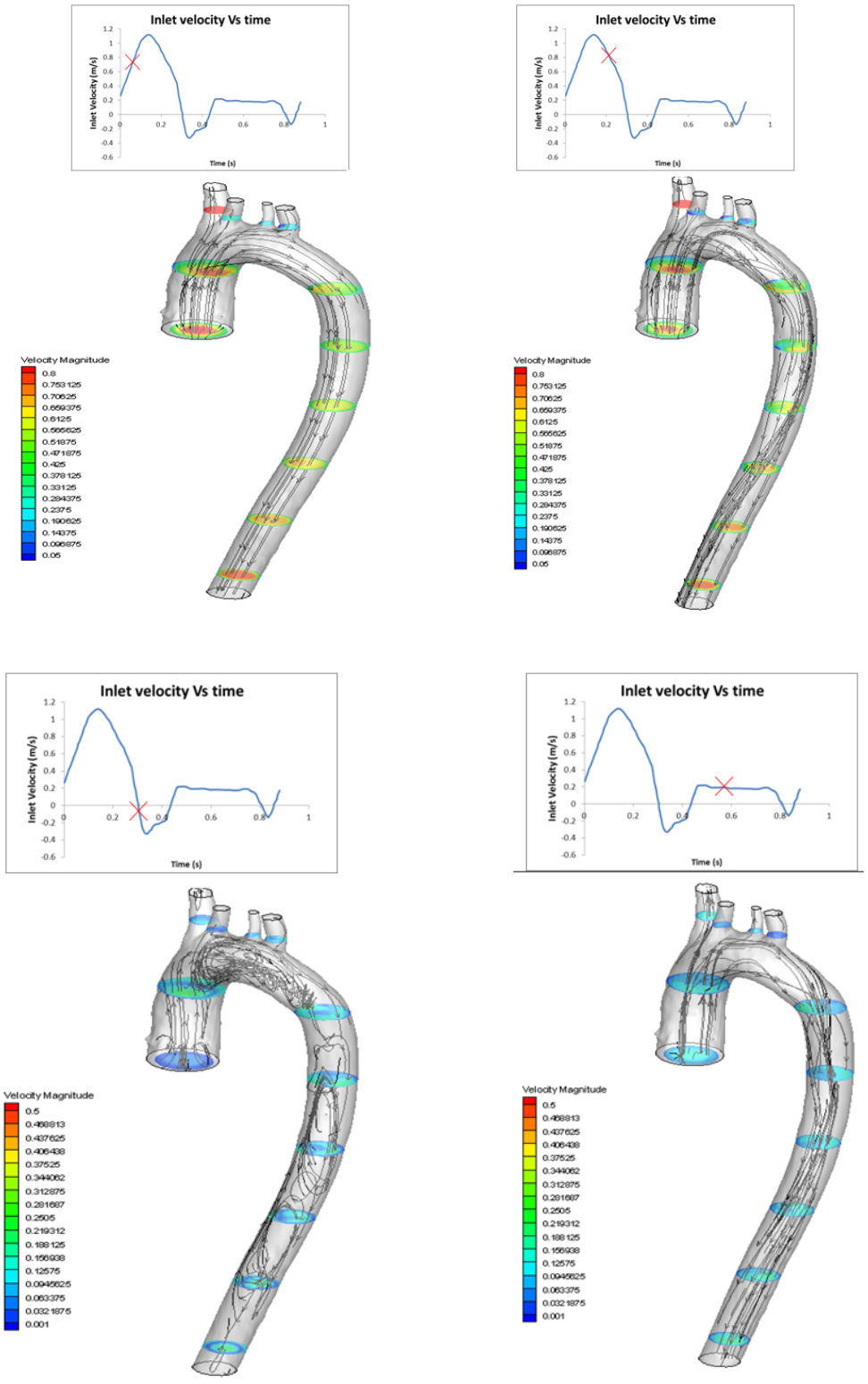

Figure 4.9. Velocity magnitude(m/s) with streamlines for four phases of cardiac cycle

The inlet pulsatile velocity profiles show that during peak flow the velocity increases to a high value that results turbulent flow (Re >2000) within the aorta. In the present work, the flow turbulence is modeled by $k-\epsilon$ turbulence model (since it is computationally cheap and easy to implement) that can account for the turbulence effects at the inlet which was not required in steady flow simulation.

From the streamline profile of the deceleration phase (Fig: 4.9) we can see a helical flow profile of blood as it is flowing from the anterior part to the posterior part of the aorta. Due to sudden negative flow velocity through the inlet, vorticity originates at the arch and descending part. Again in the diastolic phase of the cardiac cycle, flow moves at a very slow speed from the inlet opening to the outlets.

In the next part we look forward for the effect of WSS at different points of pulsatile flow rate at the inlet. In Fig: 4.10, it is shown that during peak systolic flow the subclavian artery has the highest shear stress and WSS is also high at the roots of all branches. This is because the high flow velocity starting at the inlet has the maximum flow passing through the nearest exit, leaving a considerably high amount of WSS at that region.

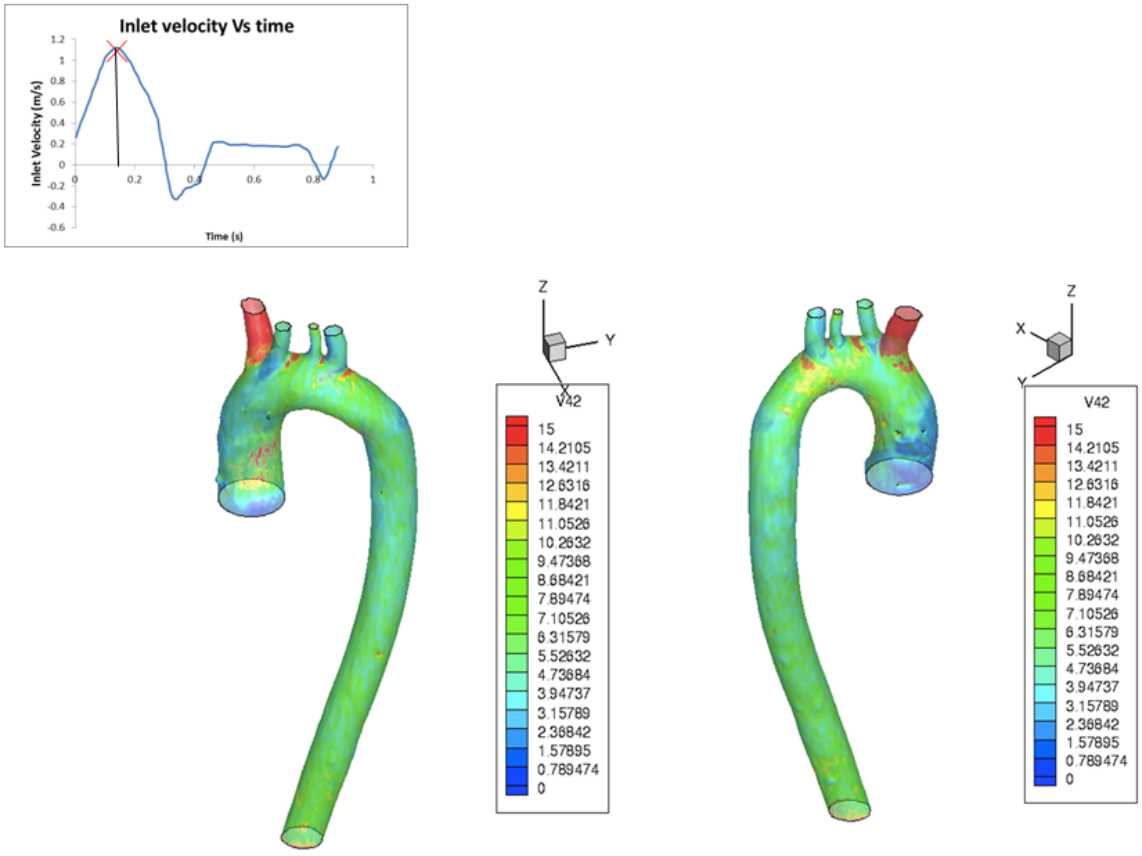

Figure 4.10. WSS(Pa) at the time of peak systolic flow (t = 0.15s) for anterior (left) and posterior (right) part of normal Aorta

At the time of max deceleration (Fig: 4.11), the flow rate is minimum (almost zero) resulting in a very small amount of WSS at that region. Comparatively higher WSS is found at the inner curvature of the thoracic aorta and the descending aorta since the fluid has not left the part yet, and that is why as we go down the descending aorta part, WSS keeps increasing.

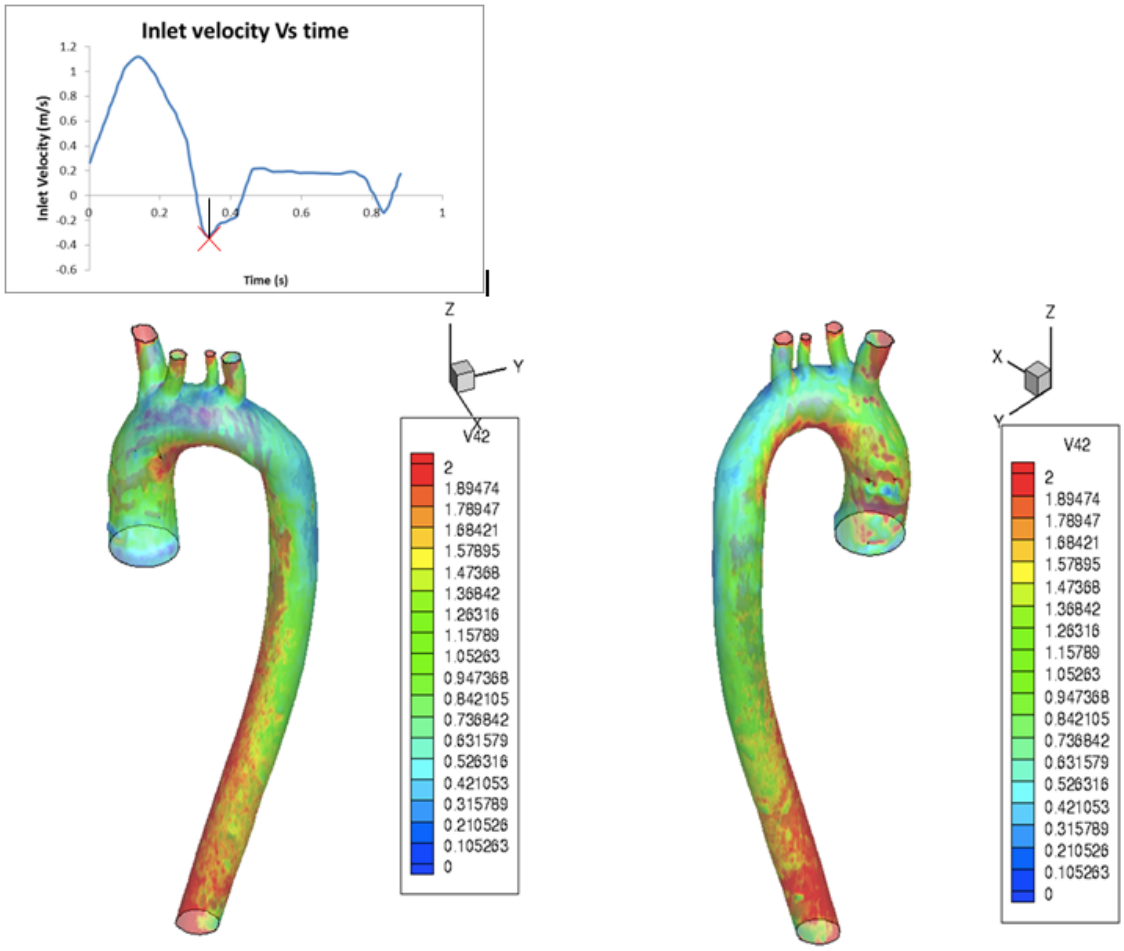

Figure 4.11. WSS(Pa) at the time of maximum deceleration (t = 0.37s) for anterior (left) and posterior (right) part of normal aorta

Again at time 0.52s we observe a slight increase of flow velocity, creating the same WSS pattern, like peak systolic flow though the value of WSS is much lower than it was during peak systolic flow.

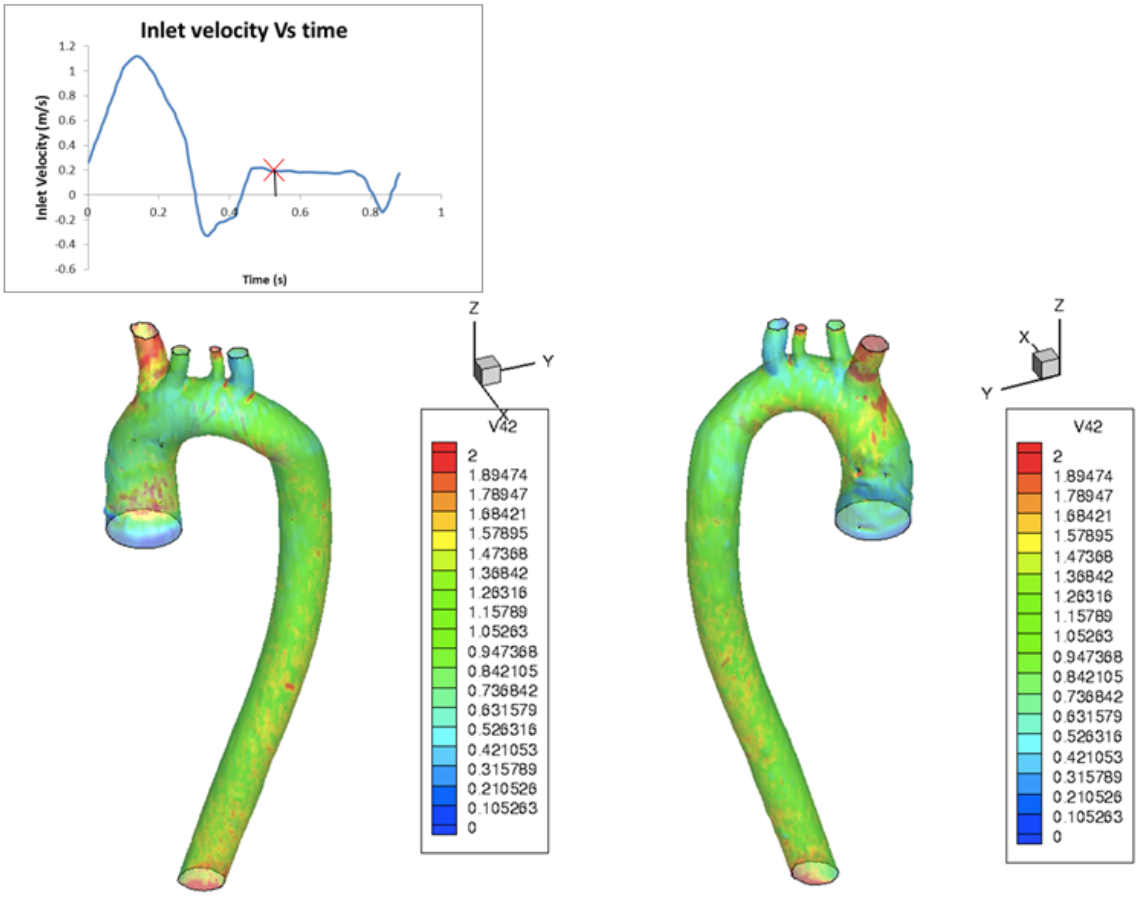

Figure 4.12. WSS(Pa) at the time of mid-diastole deceleration (t = 0.52s) for anterior (left) and posterior (right) part of normal aorta

Now at the diastolic phase,which is the last phase of the flow (Fig: 4.12), flow reversals occur. Since in this case flow is moving out of the inlet, backflow from the descending part to the ascending part occurs resulting in higher values of WSS at the branches. Random streamlines are formed resulting in sporadic WSS generation at different regions of the aortic wall. WSS at the end part of the descending aorta is higher due to high backflow and the turbulent nature of the flow.

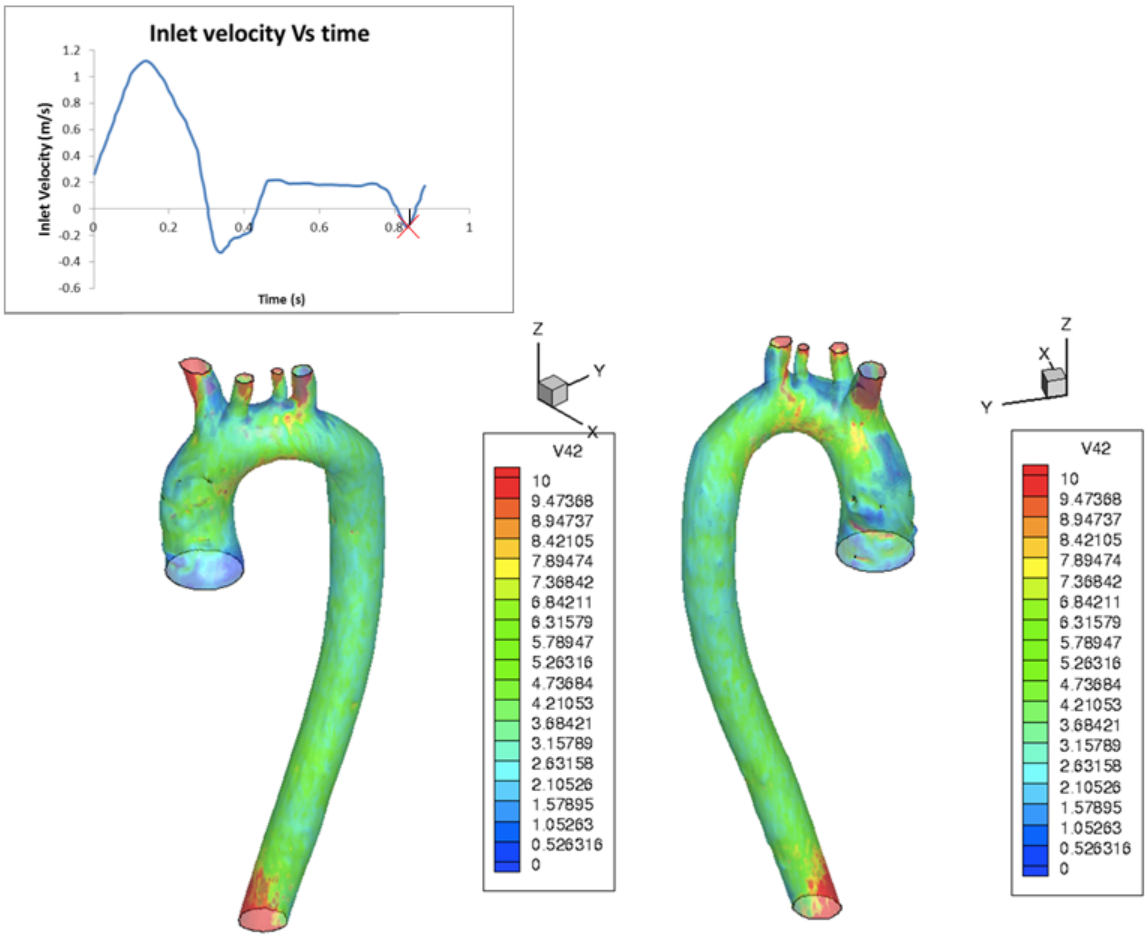

Figure 4.13. WSS(Pa) at the time of end diastole period (t = 0.85s) for anterior (left) and posterior (right) part of normal aorta

In similar fashion, the WSS distribution was also examined for the diseased aorta to find the weak regions that are prone to aortic diseases like aneurysm or aortic dissection.

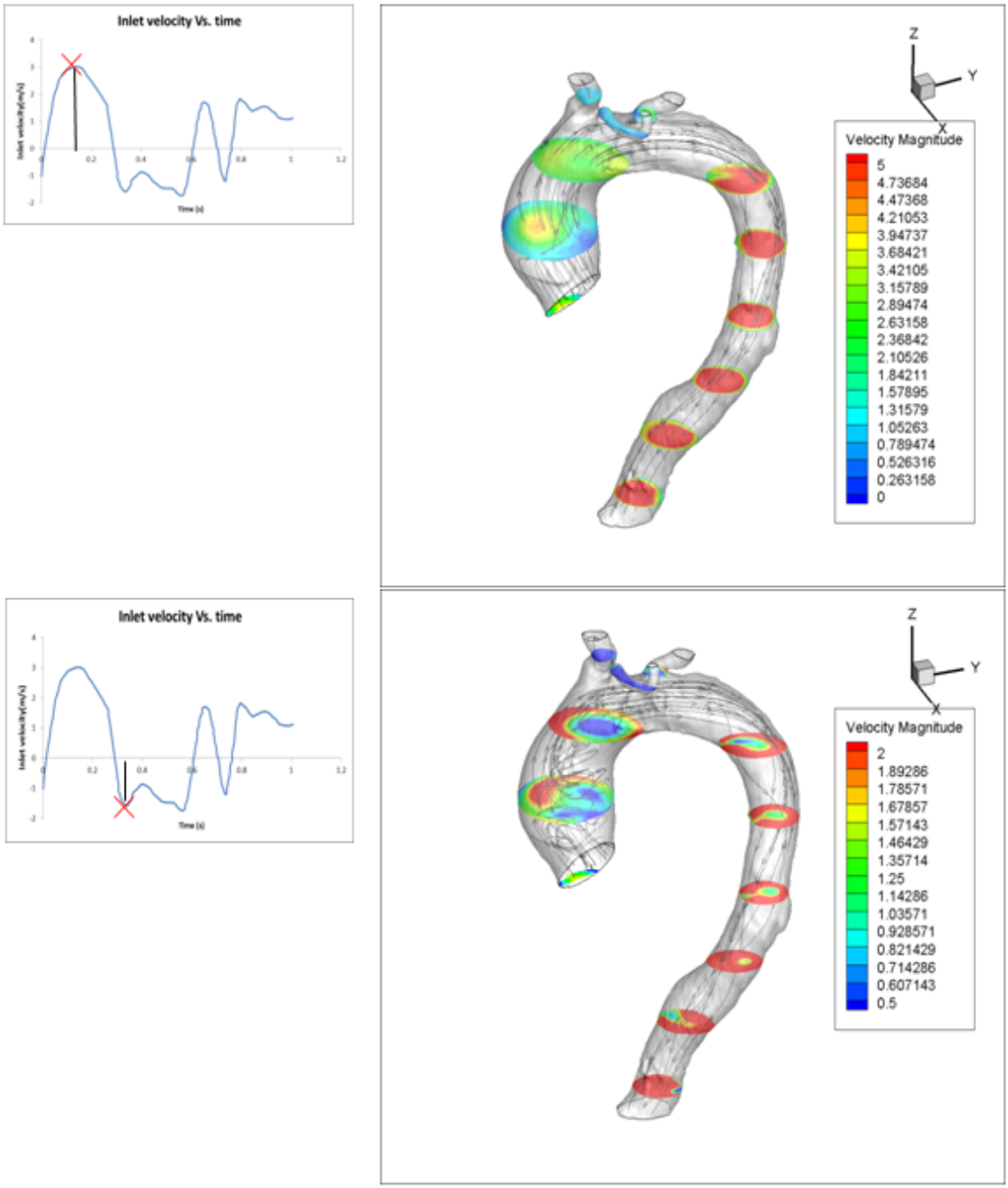

Figure 4.14. Velocity magnitude(m/s) with streamlines for peak systolic and diastolic phases of the cardiac cycle

In Fig: 4.15, the peak systolic period was represented which necessarily displayed high WSS values at the aortic arch and branch root regions. However, sporadic low WSS values were found which definitely represented the presence of flow circulation in those regions.

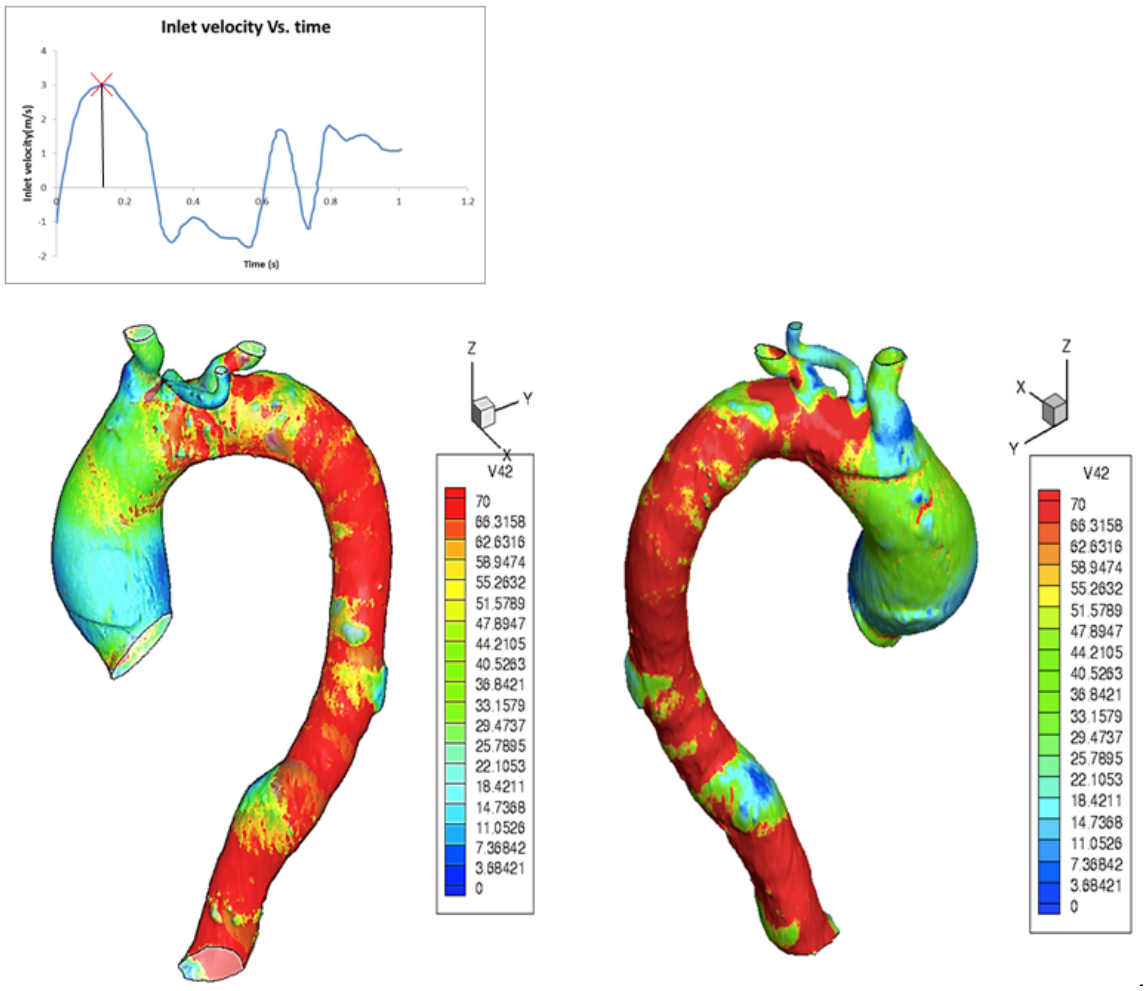

Figure 4.15. WSS(Pa) at the time of peak systole period (t = 0.18s) for anterior (left) and posterior (right) part of dilated aorta

In the period of peak diastolic deceleration (t = 0.37s) a very low amount of flow passes through the branches (Fig: 4.16) since inlet velocity is not high enough to drive

the flow through the narrow branches. Thus high WSS generates near the aortic roots and the aortic arch and the descending part of the aorta.

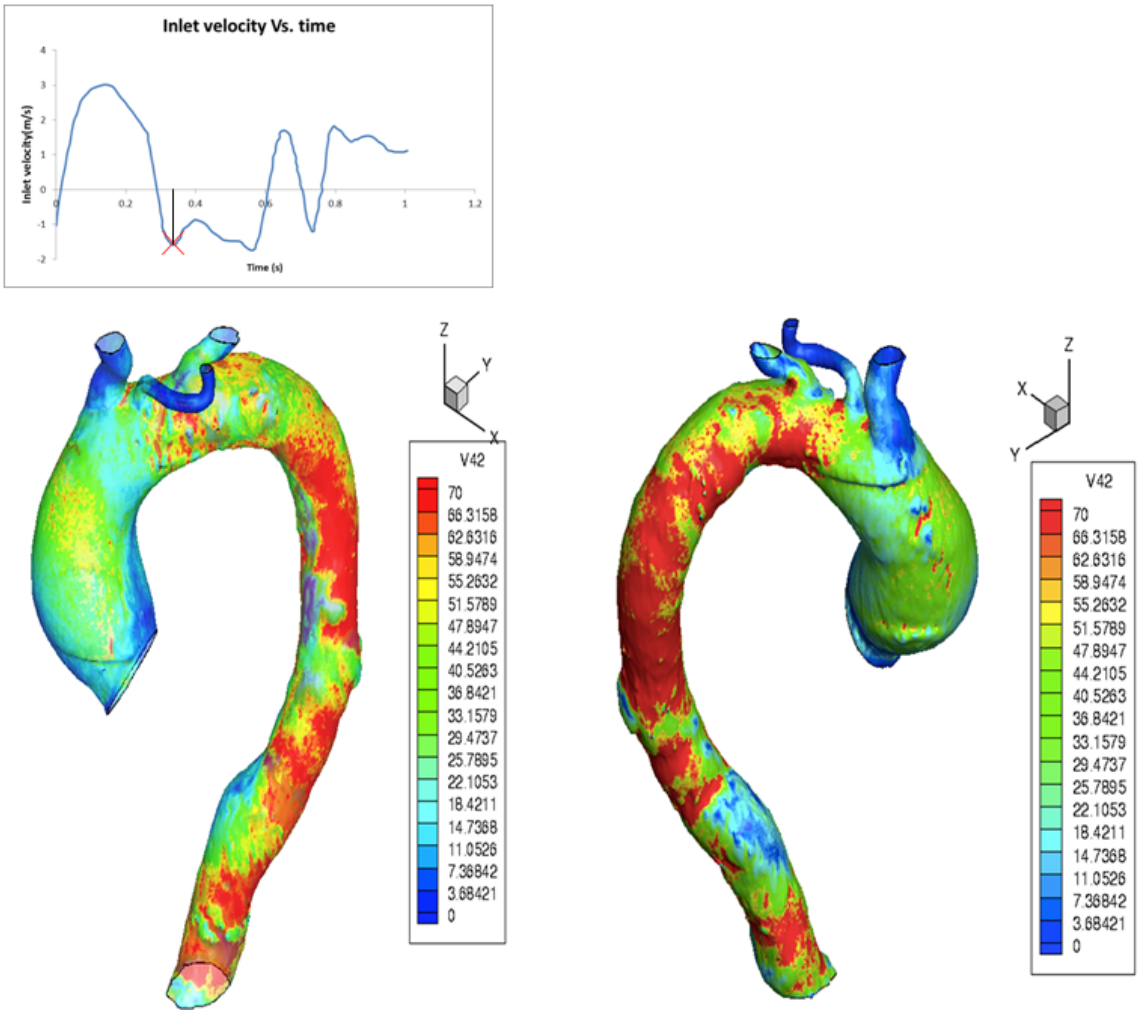

Figure 4.16. WSS(Pa) at the time of peak systolic period (t = 0.37s) for anterior (left) and posterior (right) part of dilated Aorta

While the flow increases once again, flow gets past the branches, generating higher WSS at the branches themselves. However, during all these time phases a strange phenomenon is observed near the outlet of the descending aorta part. Irrespective of all flow regimes, a low shear stress region is developed there. Vorticial effect is

definitely there, but the reason behind the exact flow phenomena still needs some further investigation.

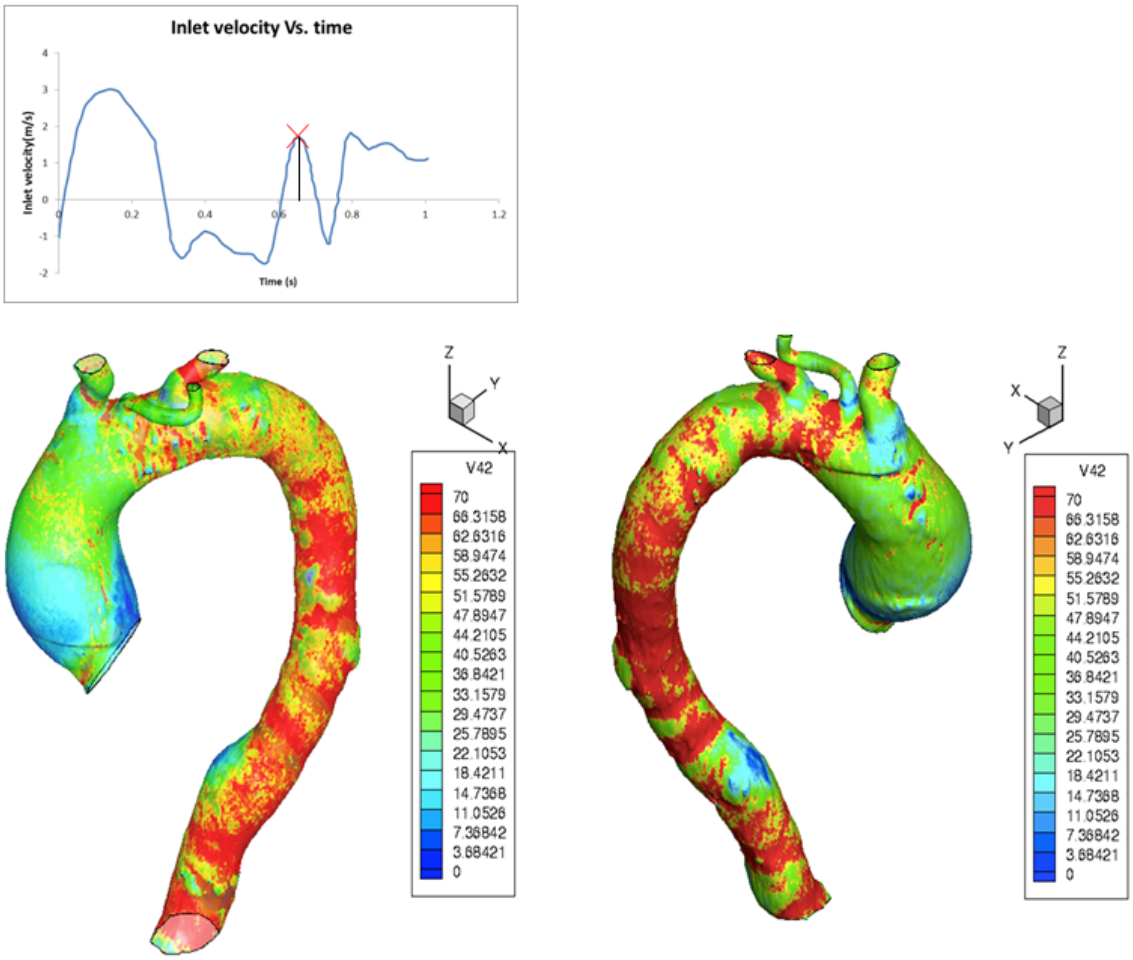

Figure 4.17. WSS(Pa) at the time of 0.37s for anterior (left) and posterior (right) part of dilated Aorta

Some common features of these flow phenomena can be validated from some previous research for simplified aortas. N. Shahcheragi et. al. [26] demonstrated high WSS at branch roots for both diastolic and systolic phases of the cardiac cycle that is evident in our results. Moreover, during a diastolic (decelerating) phase analysis for different inlet boundary conditions, Manasori et.al [30] also discovered high WSS at the lower aortic arch for all conditions. Our results also display the same (Fig:

4.18, 4.19) for diastolic phase analysis of the cardiac cycle. Moreover, These results confirm the accuracy of the fluid modeling methodology we used in our simulation to proceed further accordingly.

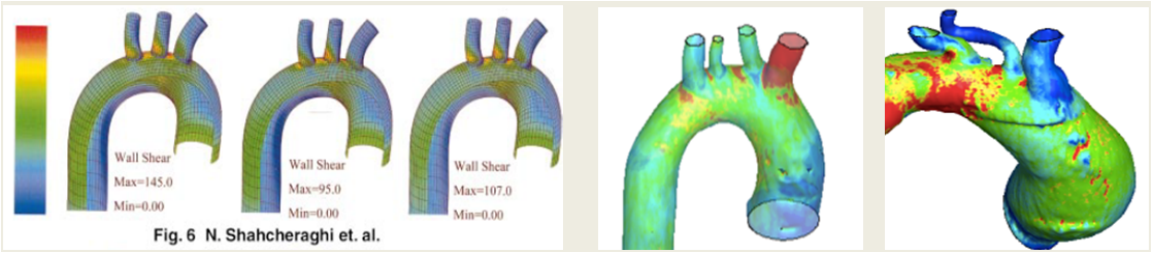

Figure 4.18. WSS(Pa) validation at the branch roots for peak diastolic phase

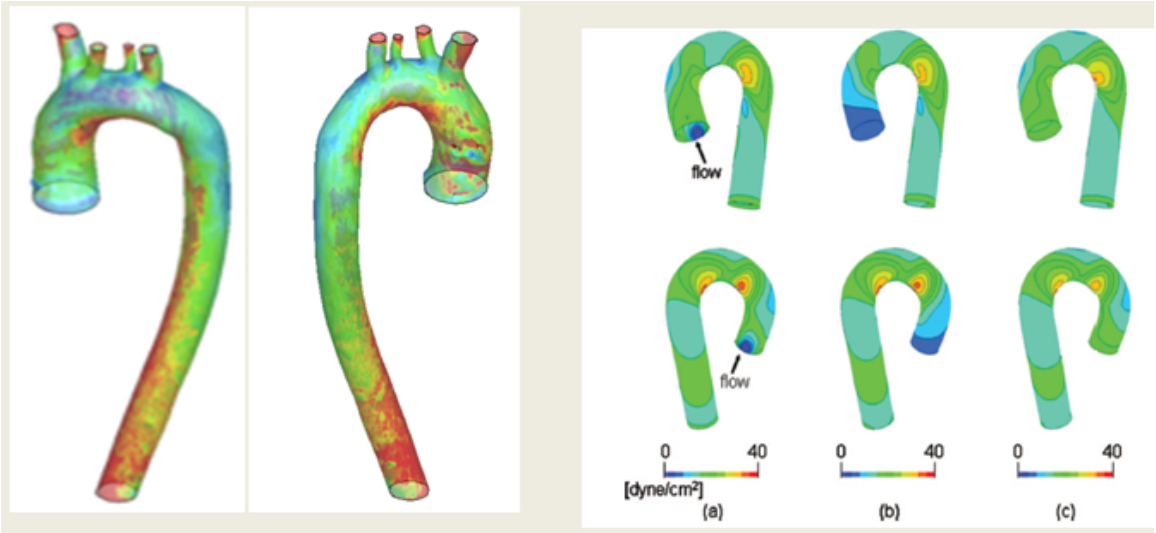

Figure 4.19. WSS(Pa) validation at lower aortic arch region for peak diastolic phase

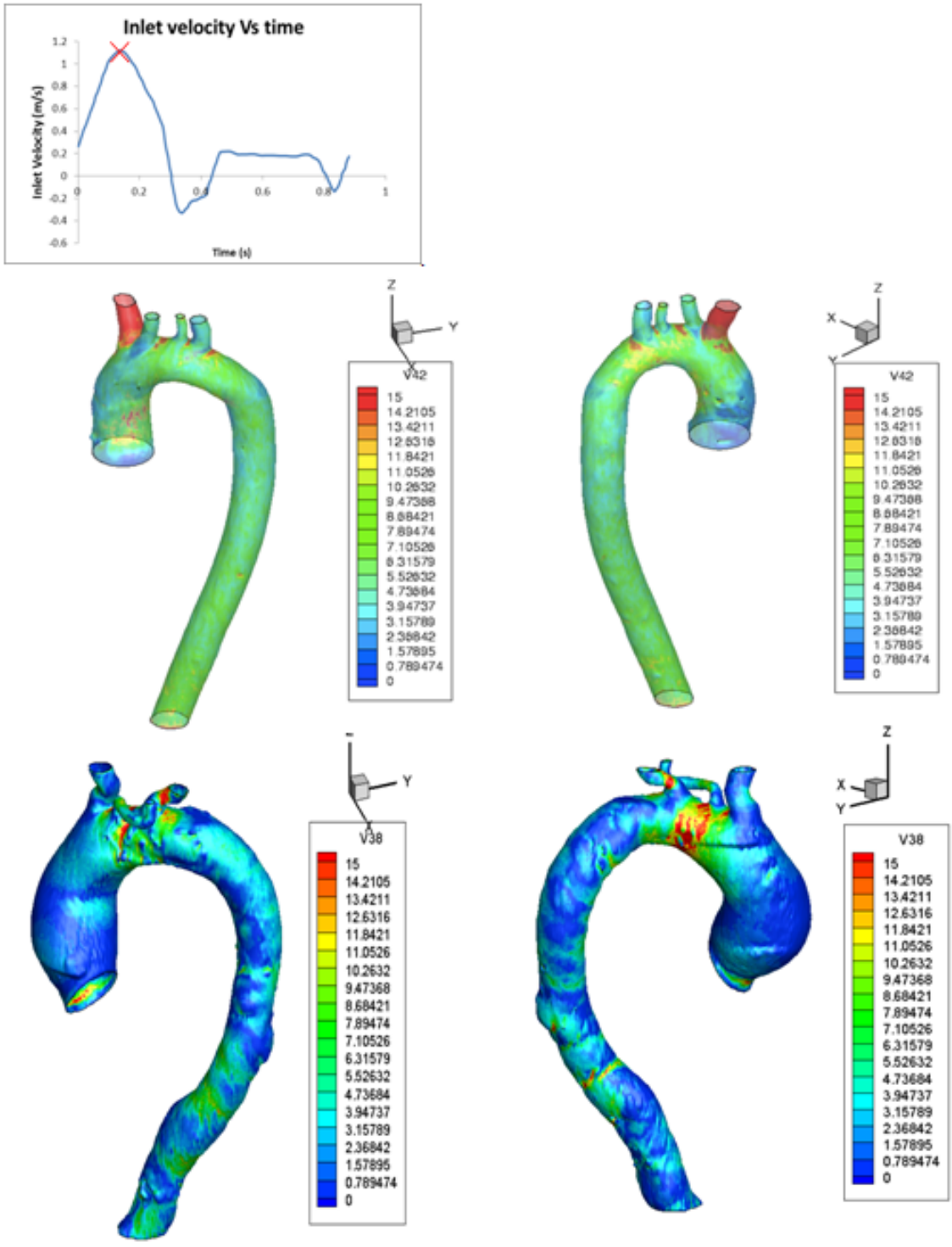

Figure 4.20. WSS(Pa) comparison for peak systolic flow

WSS comparisons for pulsatile analysis results between the normal and the dilated aorta are performed afterwards. Similar pulsatile flow profiles (normal aortic flow) were assumed at the inlets. For peak systolic flow (Fig: 4.20), the dilated aorta displayed lower WSS at the ascending aorta region. Due to dilation, the velocity was lower at the ascending part of the aorta resulting in lower WSS.

For other phases of the pulsatile flow, a higher value of WSS was observed at dilated aortic wall than normal aortic wall. Moreover, a more sporadic distribution of WSS was found in the dilated aorta. Like previous findings, lower inlet flow rate resulted in lower value of WSS whereas higher WSS was generated in the case of peak systolic flow for both normal and dilated aortas.

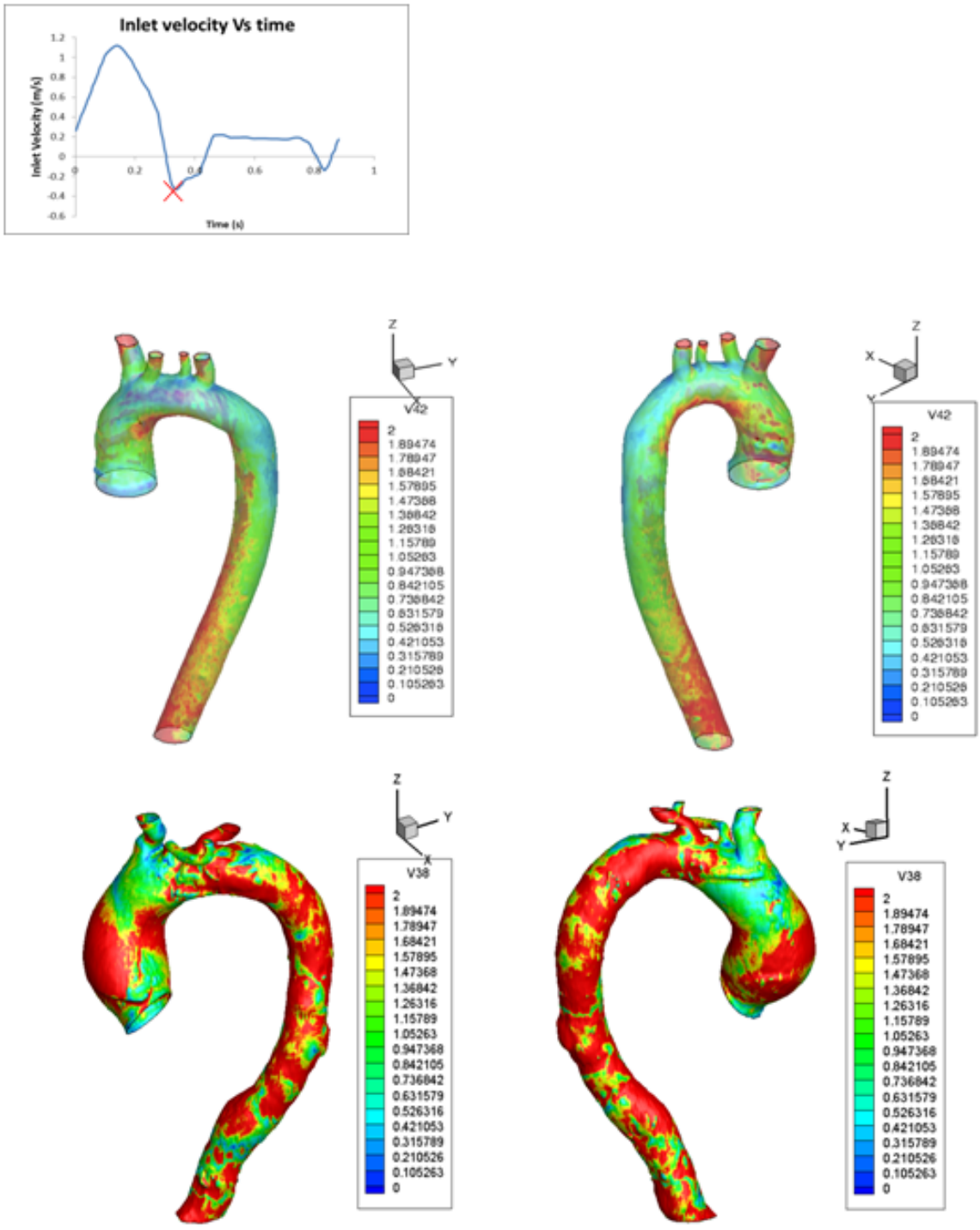

Figure 4.21. WSS(Pa) comparison for flow diastole

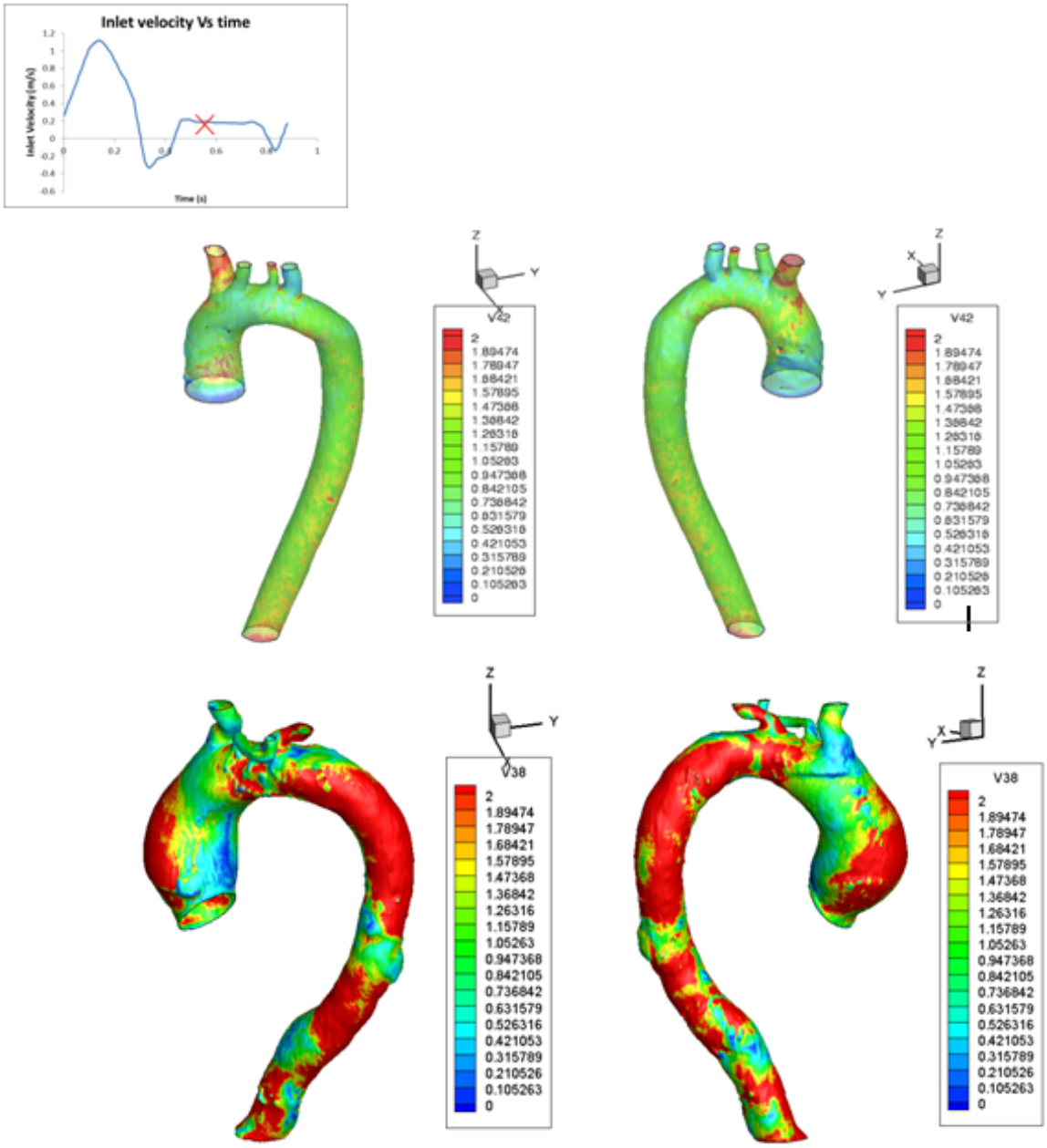

Figure 4.22. WSS(Pa) comparison for mid diastole flow

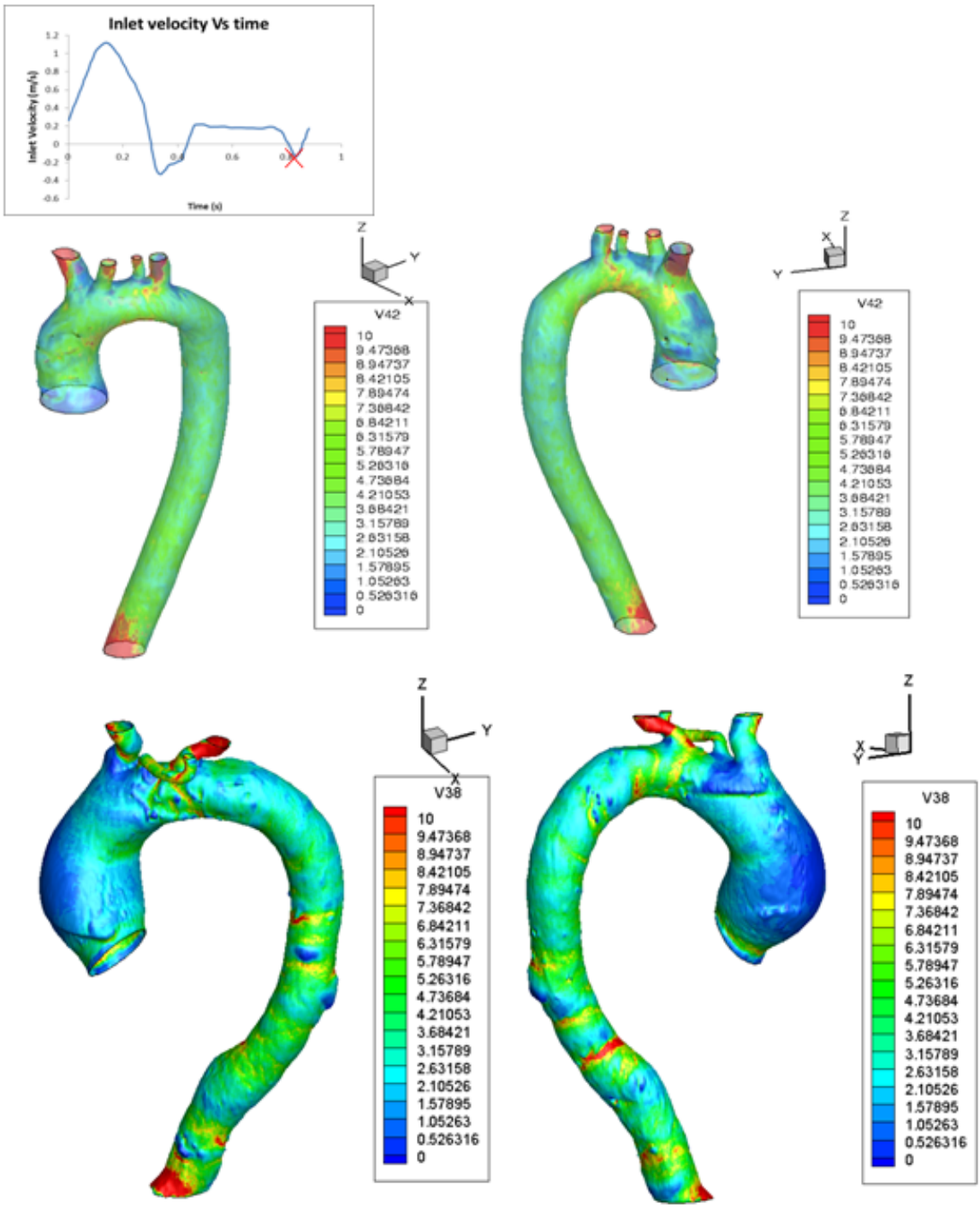

Figure 4.23. WSS(Pa) comparison for end diastole flow

Velocity skewness comparison was also performed for both normal and dilated aorta for peak systole (Fig: 4.24) and diastole (Fig: 4.25) of the cardiac cycle. For peak systolic flow, lower velocity magnitude was obtained in the dilated aorta at the ascending part because the diameter of that region was larger, but at the descending part the velocity eventually got higher. For both the cases, velocity skewness was found at the arch regions of the aortas.

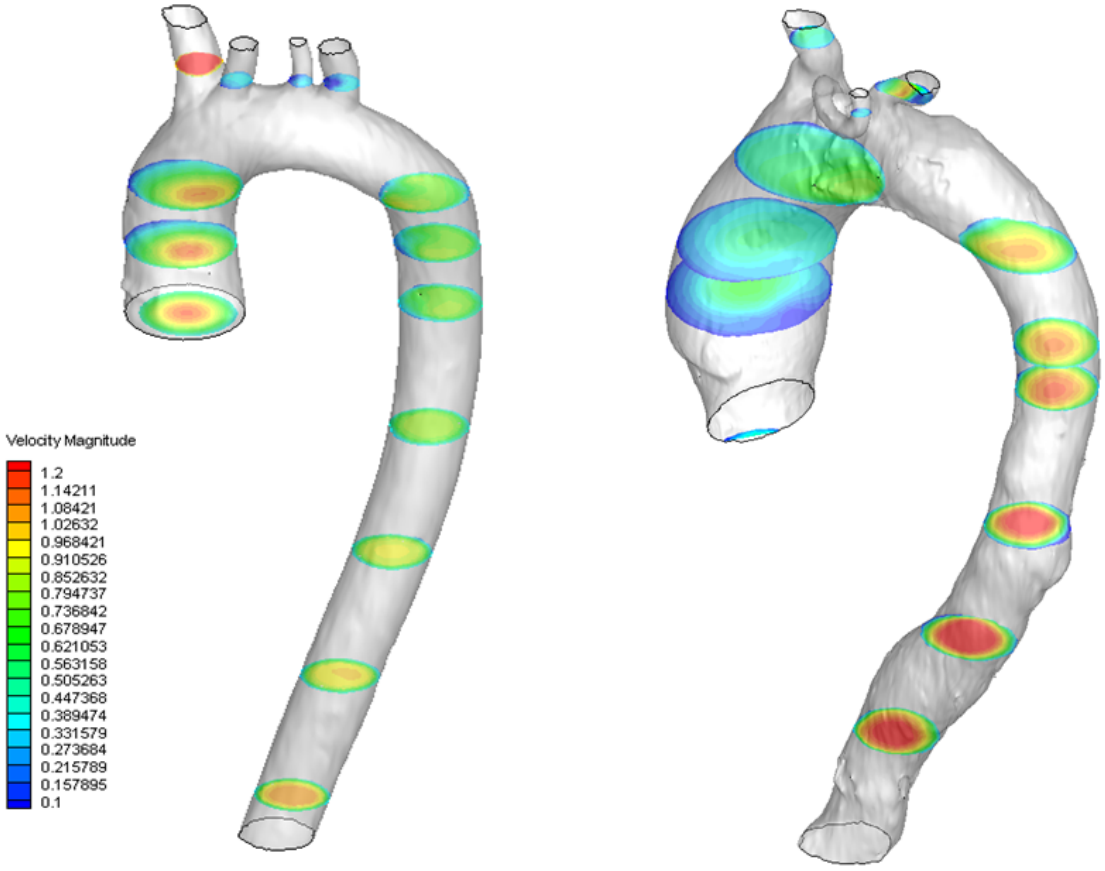

Figure 4.24. Velocity(m/s) profile comparison for normal and dilated aorta at peak systole

For the diastolic phase, the skewness was observed near the aortic arch regions in a fashion similar to the systolic phase. Backflow was happening in this case and

random vortices were created generating erratic flow patterns which were described previously.

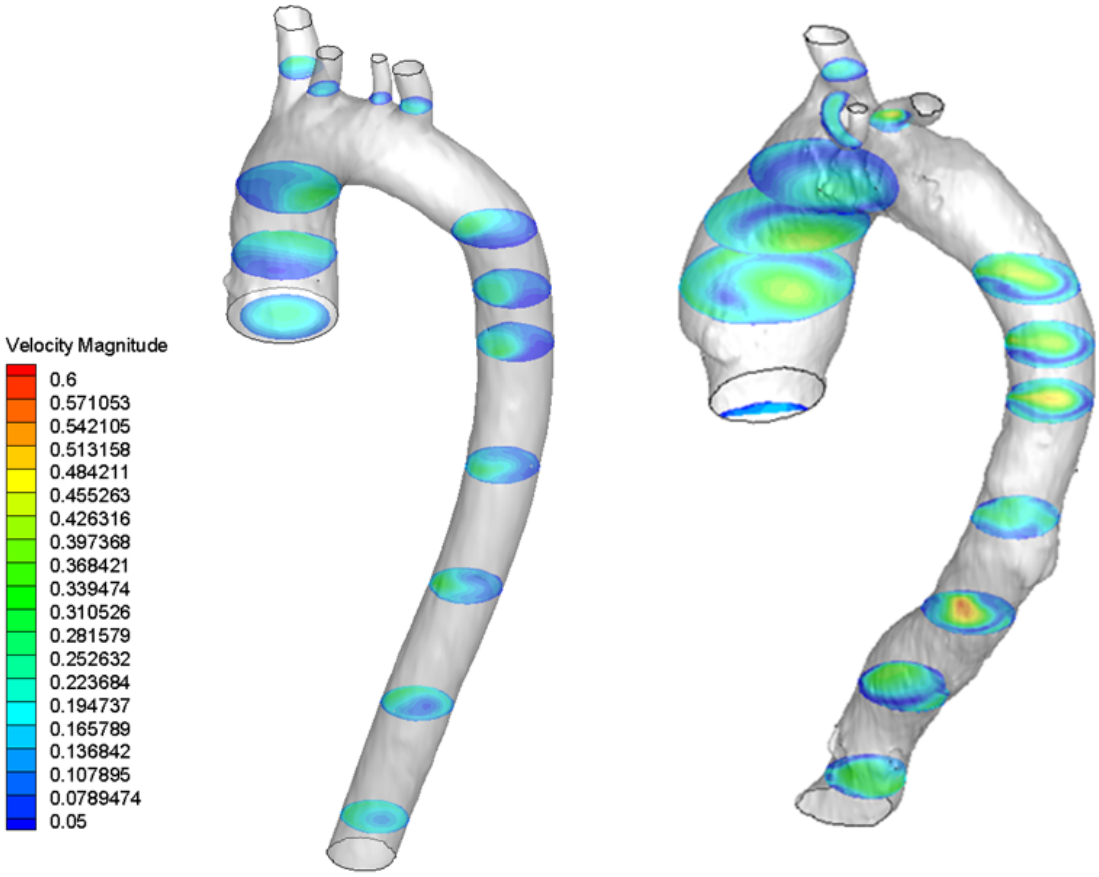

Figure 4.25. Velocity(m/s) profile comparison for normal and dilated aorta at peak diastole

5. PRELIMINARY RESULTS OF FLUID-STRUCTURE INTERACTION (FSI) SIMULATION OF AORTA USING ANSYS-WORKBENCH

Fluidstructure interaction (FSI) is the interaction of some movable or deformable structure with an internal or surrounding fluid flow. The interaction between fluid and structure occurs in a wide range of engineering problems. The interaction between fluids and solids is a phenomenon that can often be observed in nature, for example, the deformation of trees or the movement of sand dunes caused by wind. In almost the same manner, wind can interact with buildings, sometimes with dramatic consequences, such as the collapse of the Tacoma-Narrows Bridge in November 1940. The solution for such problems is based on the relations of continuum mechanics and is mostly solved with numerical methods. It is a computational challenge to solve such problems because of the complex geometries, intricate physics of fluids, and complicated fluid-structure interactions. Solution strategies for FSI simulations are mainly divided into monolithic and partitioned methods; this section will focus only on partitioned methods [20] since the package used for the simulation purpose here is ANSYS Workbench that follows the same methodology.

5.1 Methodology

Regardless of whether one-way or two-way coupling methods are used, the solutions are based on a partitioned method where separate solutions for the different physical fields are prepared. One field that has to be solved is fluid dynamics, the other is structure dynamics. At the boundary between fluids and solids, the fluid-structure interface, information for the solution is shared between the fluid solver and structure solver. The information exchanged is dependent on the coupling method. For one-way coupling calculations, only the fluid pressure acting at the structure is

transferred to the structure solver. For two-way-coupling calculations, the displacement of the structure is also transferred to the fluid solver.

In the top part of Fig: 5.1 procedure is shown for one-way coupling. Initially, the fluid field is solved until the convergence criteria are reached. The calculated forces at the structure boundaries are then transferred to the structure side. Next, the structure side is calculated until the convergence criterion is reached. Then, the fluid flow for the next time step is calculated to convergence. The solution is finished when the maximum number of time steps is reached.

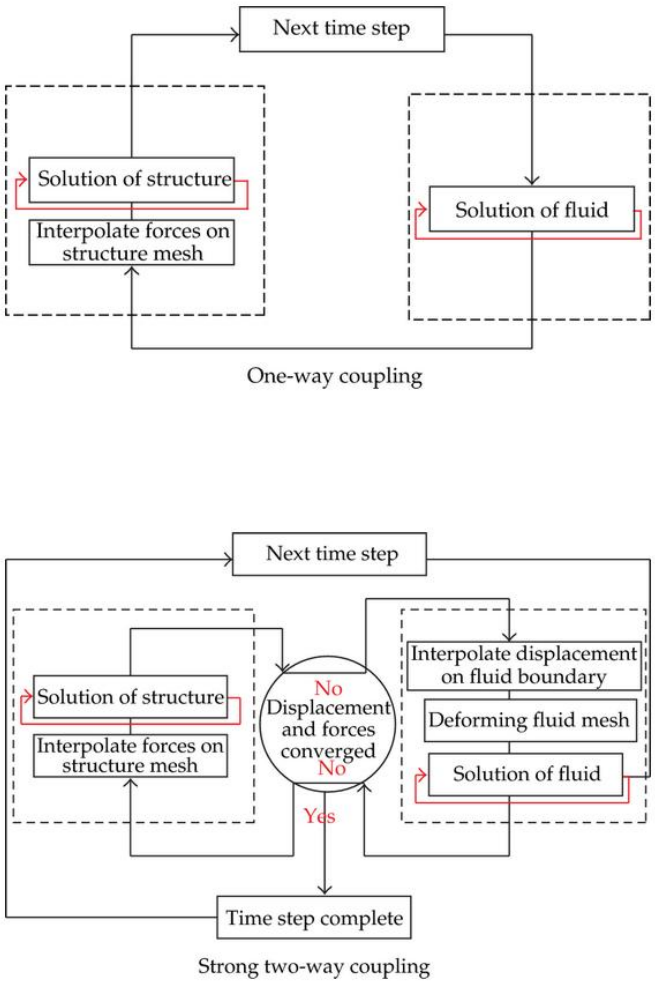

Figure 5.1. Solution algorithm for one and strong two-way coupling [20].

The process flow chart for the strong two-way coupling algorithm is shown on the bottom of Figure 5.1. Within one-time step during the transient simulation, a converged solution for the flow field is required to provide the forces acting on the body. After interpolating the forces from the fluid mesh to the surface mesh of the structure, a converged solution of the structural dynamics will be attained under the effect of the acting forces. The response of the structure to the emerging load represents a displacement of the structural grid nodes. The displacements at the boundary between structure and fluid are interpolated to the fluid mesh which leads to its deformation. This step closes one inner loop of the simulation. For strong two-way-coupling simulations, these steps are repeated until the changes in the flow forces and the structural displacements fall below a prescribed amount. Afterwards, a new time step is launched. For weak two-way coupling simulations, the convergence at the boundary between structure and fluid is not considered and a new time step is launched directly.

Application-wise, FSI simulation can be categorized likewise in Fig: 5.2.

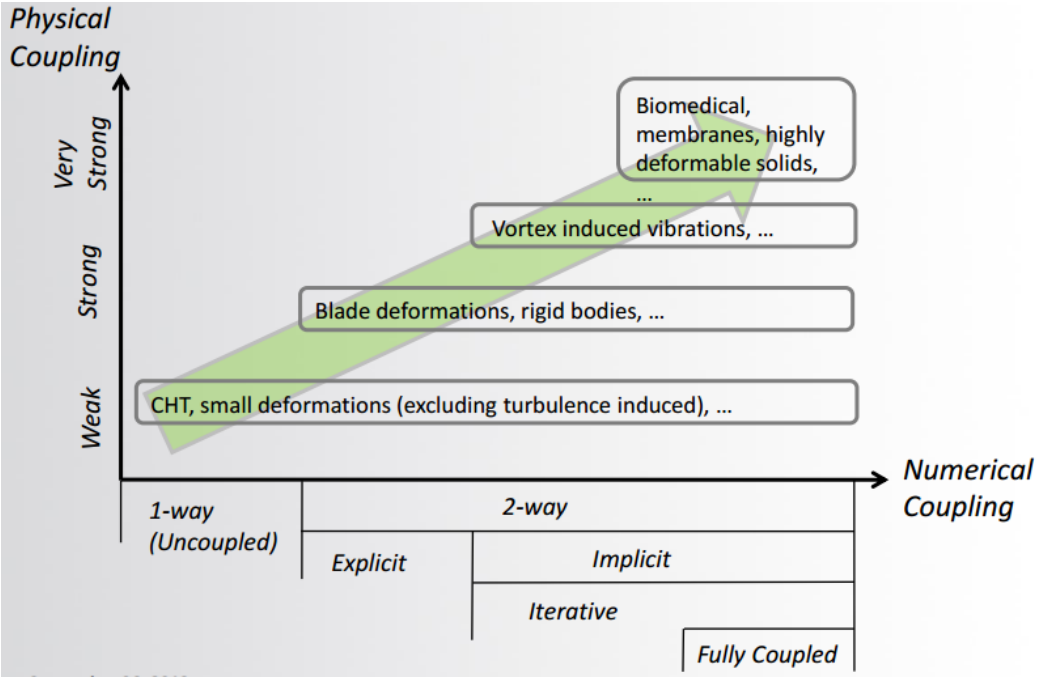

Figure 5.2. Application based categorization of FSI simulation [21].

Some general comments can be made about both methods. Often the advantage of one method is a disadvantage of the other. In general, the two-way coupling solution is more accurate, especially for larger deflections where the fluid field is strongly influenced by structural deformation. Strong two-way coupling solutions can be of second-order time accuracy and are more stable (see Vaassen et al. [21]). The one-way coupling method does not guarantee energy conservation at the interface, but two-way does. A benefit of one-way coupling simulation is significantly lower computational time. A second benefit is that deformation of the fluid mesh does not need to be calculated, which provides a mesh of constant quality.

5.2 FSI Modeling and Simulation of Normal Aorta

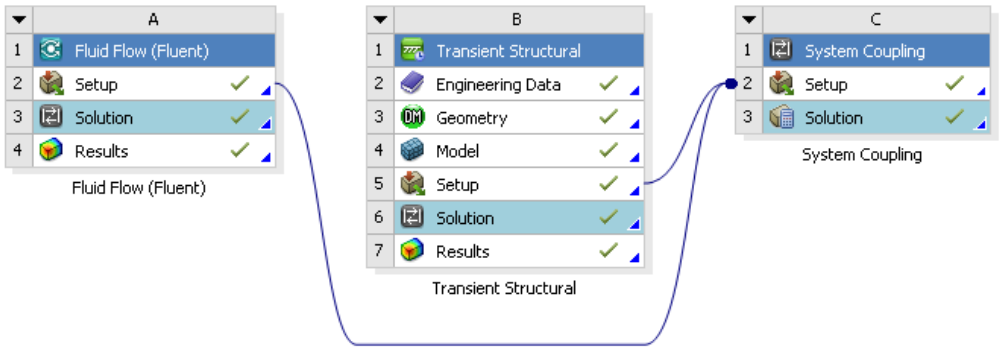

Figure 5.3. Flowchart of the coupling analysis (Courtesy: Ansys Workbench)

The figure above describes the schematic of the FSI simulation performed in Ansys. Module A represents the fluid flow analysis, module B solid structural analysis and module C is used to couple the simulation to get the FSI results.

The aorta is comprised of a three-layered wall [16] with different values of Youngs moduli,but in our case we took a mean total thickness of 2.5mm with a mean value of Youngs modulus of 2.7 MPa and a density of 2000 kg/m^3. At the aortic inlet, a flat flow velocity profile was used with the peak velocity ($1.1m/s$) of the cardiac cycle and the wall was considered as no-slip. The assumption of a flat velocity profile at the aortic inlet is justified by in vivo measurements using hot film anemometry on various animal models that have demonstrated that the velocity profile distal to the aortic valve are relatively flat, Nerem [21].

Boundary Conditions: The surfaces of the aortic inlet and the aortic outlets with the branches are fixed in all directions. The other outer surface of the aortic model was taken as load free fluid solid interface (Fig: 5.4). The fluid boundary condition was the same as steady flow simulation case.

The simulation was performed for unsteady flow analysis and since the geometry was highly complicated and mesh was highly skewed; a very low time step and coarse mesh of fluid part was chosen for better mapping at fluid solid interface region. A very low time step of $1.0e-5s$ was chosen and the simulation ran for 12 time steps. $k-\epsilon$ turbulent model was chosen as the viscous mode(since the peak velocity results in turbulent flow from the very beginning) with PISO (Pressure-Implicit with Splitting of Operators) algorithm as pressure velocity coupling to improve the efficiency by performing neighbor correction and skewness correction. The FSI simulation in this work was just an attempt to simulate the blood flow using Ansys Workbench since it only ran for 12 time steps. High skewness of the mesh resulted in divergence of the results after that time step. Thus the results presented here is to see the qualitative nature of the blood flow at the very initial stage. A more extensive study needs to be done here to represent the actual blood flow phenomena according to the actual flow case.

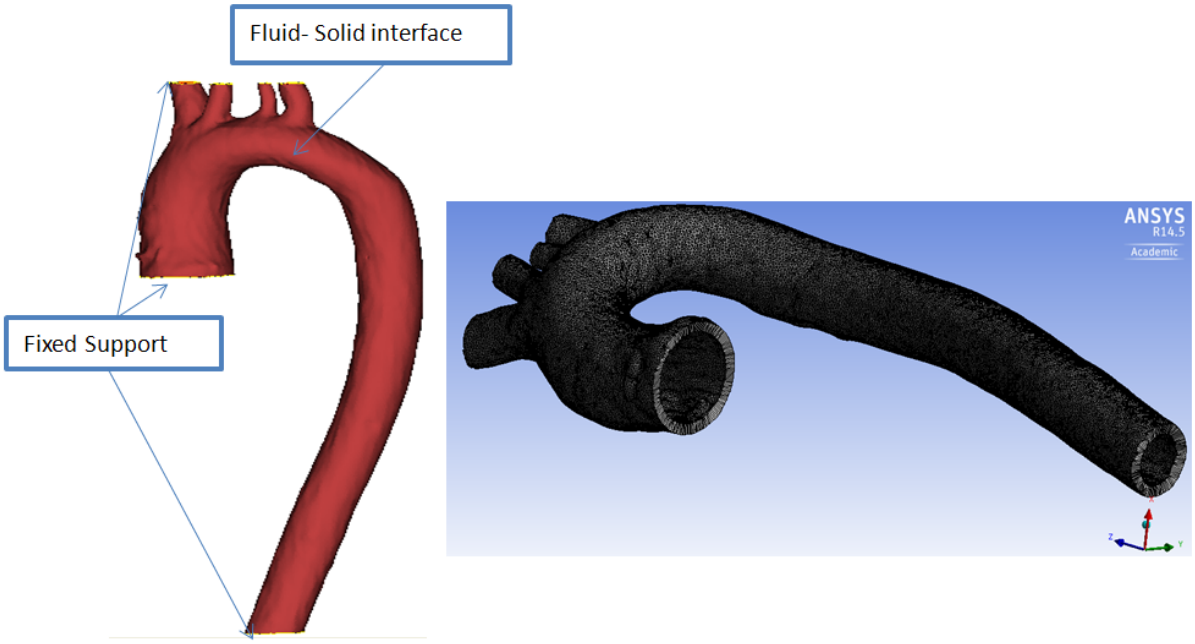

Figure 5.4. Skin of the Aorta with structural boundary conditions (left) and with the thickness of 2.5mm (right)

Deformation is defined by the change in the shape or size of an object due to an applied force. It can be resulted due to tensile, compressive, shear bending or torsion. While displacement determines the a vector extending from a particle's initial location to its deformed location; deformation is determined by a deformation gradient tensor that quantifies the changes in co-ordinate vectors from original position.

From the contours of deformation of the aorta (Fig: 5.5) we can see that a large amount of deformation is occurring at the aortic arch and the branch roots of the aorta.

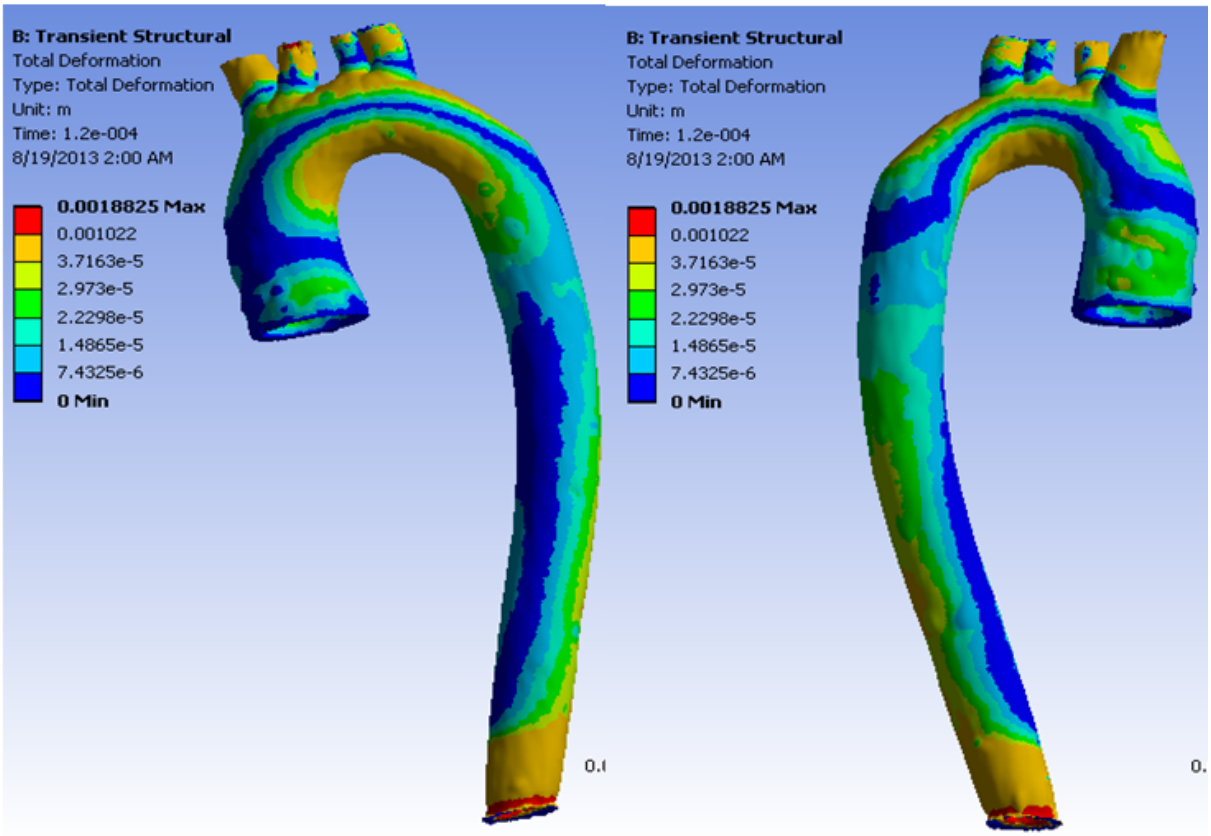

Figure 5.5. Deformation of Aorta at cardiac cycle peak velocity of 1.1m/s, Anterior view(left), posterior view (right)

As we continued our study to find out the maximum equivalent (Von-Mises) stress (Fig: 5.6), we also realized that a high amount is generated at the aortic arch and for similar reasons described beforehand.

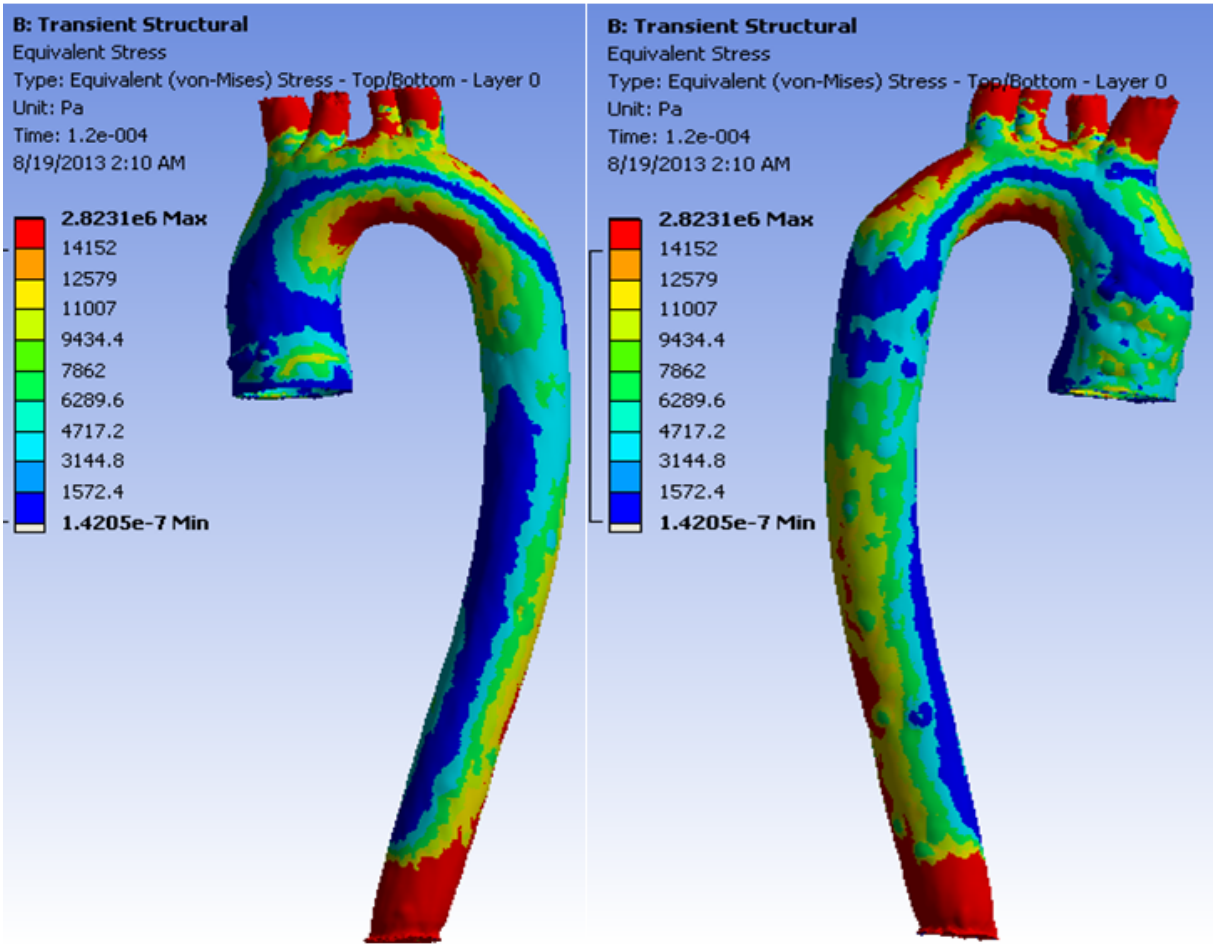

Figure 5.6. Equivalent (Von Mises) Stress of Aorta at cardiac cycle peak velocity of 1.1m/s, Anterior view (left), posterior view (right)

The major limitation of the FSI simulation was, it was only performed for the peak velocity of the cardiac cycle; disregarding the pulsatile tendency of the inlet velocity. The reason was the computational expense was way above the capacity of the machine to complete the work within required time frame. That's the same reason behind not performing the FSI simulation of the dilated aorta as well.

6. DISCUSSION AND FURTHER WORK

Dilation of Ascending Aorta entails a high risk of dissection or aortic rupture in the absence of surgical treatment. Aortic aneurysms remain the 13th leading cause of mortality in western countries. The incidence of thoracic aortic aneurysms is estimated to be 4.5 cases per 100000. Supravalvular aortic aneurysms are less common, and predominantly affect male patients (ratio 3:1); the mean age at the time of diagnosis ranges from 59 to 69 years. In the case of aortic root aneurysms, patients are younger (30 to 50 years), with a 1:1 sex ratio [30]. Preventive measures can be taken beforehand if dilation prone locations can be identified and treated accordingly. Thus, blood flow analysis for the whole cardiac cycle analysis is necessary to find these regions accordingly.

On this line, our research helps in finding locations where high WSS was generated giving rise to the fact that high wall shear stress is the predominant factor in determining the regions of several arterial wall diseases. Hence risk of diseases like wall dissection and rupture can be significantly reduced if we can identify the risk regions and take measures accordingly. This study was specifically important because previous studies did not include an exact model of the real patient aorta by smoothing out the geometry significantly to ease the mesh as well as the solution or excluding the branches to reduce complexity of the geometry.

Modeling this problem, though straightforward, was full of technical ventures. Most of the previous simulation used simplified geometry for modeling and simulation of the blood flow scenarios, but this research comprised of an actual aorta from patients without compromising the geometric complexities. Also to our knowledge,the attempt to FSI simulation using Ansys Workbench for this case has not been performed beforehand. Thus, the research showed a path to find out the higher WSS and deflected areas accordingly.

The results of the steady flow simulations have revealed a flow field that is largely similar as described in Chapter 3 of the thesis that demonstrates that the results of the simulations are credible. Thus, the simulations performed for pulsatile case can only be referred to qualitative approximation of real time flow.

The results revealed that WSS values are always larger for a dilated aorta than a normal Aorta. This happens due to the fact of having more curved nature of the geometry that results in high WSS that is more prone to arterial diseases.

From the attempt to FSI simulation results, a high amount of deformation and equivalent stress is found near the arch of the aorta which resembles that the region is prone to rupture failure and physicians should take therapeutic measures accordingly to prevent further occlusion and fatalities afterwards.

In this study the results that we simulated for pulsatile blood flow of normal and dilated aorta is validated methodologically based on the steady flow simulation of a relevant paper. But more accuracy could have been attained if we could compare the same with an experimentation of actual blood flow situation within aorta. This was not feasible for the time being because of an extremely costly approach and due to more time requirement.

Also, though an actual Aorta is comprised of three layers: intima, adventitia and media that have respective thickness values and Youngs modulus values, we considered a total thickness of $2.5mm$ and E of $2.7MPa$ instead of taking them separately that leave the accuracy of results somewhat weak.

Next, the mechanical properties and thickness values vary from age to age [29]. Hence to some extent though it will not create significant difference in the results. But for more accurate patient relevant studies, these need to be taken care of in farther research.

For the fluid structure interaction simulation, for more accurate acquisition of deflection and mechanical stress distribution, pulsatile flow simulation was necessary. In our study we attempted for only cycle-peak velocity inlet but due to computational cost and time requirement pulsatile flow analysis of the same could not be imple-

mented. In future work, we also suggest doing this to get a grave insight of these important parameters.

Conclusion

The arterial wall tissue reacts to both the normal and shear stresses [21]. In particular, the wall shear stress is involved with the formation of atherosclerosis that is characterized by a narrowing of the arterial lumen due to the accumulation of fatty material. However wall shear stress is difficult to measure in vivo with a sufficient spatial resolution. Thus numerical simulations can help to predict the WSS distribution in a specific geometry of the vessel, improving diagnosis and prevention. A reliable numerical tool that carries out all the process from the patient-specific segmentation to the simulation could help a medical doctor to choose the correct therapy adapted to a specific patient. Furthermore, if the model is validated, a simulation of the WSS distribution can help to solve the inverse problem, i.e., to identify the role that WSS plays in the development of pathologies such as atherosclerosis.

LIST OF REFERENCES

LIST OF REFERENCES

[1] C.A. Taylor, M.T. Draney, J.P.Ku, D. Parker, B.N. Steele, K.C. Wang and C.K.Zarins, "Predictive Medicine: Computational techniques in therapeutic decision making," *Comput. Aided Surgery* 4 (1999) 231.

[2] R. Botnar, G. Rapptisch, M.B. Sheidegger, D. Liepsch, K. Perktold and P. Boesiger, "Hemodynamics in the carotid artery bifurcation: a comparison between numerical simulation and in vitro MRI measurements," *J. Biomech.* 33 (2000) 137.

[3] Y. Cheng, H. Oertel and T. Schenkel, "Fluid-structure coupled CFD simulation of the left ventricle flow during filling phase," *Ann Biomed. Eng.* 33, 567-576.

[4] R. Kerckhoffs, M. Neal, Q. Gu, J. Bassingthwaighte, J. Omens and A. McCulloch, "Coupling of a 3D finite element model of cardiac ventricular mechanics to lumped systems models of the systemic and pulmonic circulation," *Ann Biomed. Eng.* 35, 1-18.

[5] T. Schenkel, M. Malve, M. Reik, M. Markl, B. Jung, and H. Oertel, "MRI-based CFD analysis of flow in ahuman left ventricle: methodology and application to a healthy heart," *Ann. Biomed. Eng.* 37, 503-515.

[6] N. R. Saber, N. B. Wood, A.D. Gosman, R. D. Merrifield, G. J. Yang, C. L. Charrier, Gatehouse, P. D. and D. Firmin, "Progress towards subject-specific computational flow modeling of the left heart via combination of MRI with CFD," *Ann. Biomed. Eng.* 31, 42-52.

[7] H. Watanabe, S. Sugiura, H. Kafuku and T. Hisada, "Multiphysics simulation of left ventricular filling dynamics using fluid-structure interaction finite element method," *Biophys. J* 87, 2074-2085.

[8] D. M. McQueen, and C.S. Peskin, "A three-dimensional computer model of the human heart for studying cardiac fluid dynamics," *SIGGRAPH Comput. Graph.* 34, 56-60.

[9] M.D. Mantle, A.J. Sederman and L.F. Gladden, "Single and two phase flow in fixed bed reactors: MRI flow visualization and lattice-Boltzmann simulations," *Chem. Eng.Sci.* 56 (2001) 523.

[10] Y. Nakashima, Y. Watanabe, "Estimate of transport properties of porous media by microfocus X-ray computed tomography and random walk simulation," *Water Resour. Res.* 38 (2002) 1272.

[11] J. Lantz, R. Grdhagen and M. Karlsson, "The concept of aortic replacement based on computational fluid dynamic analysis: patient-directed aortic replacement," *Water Resour. Res.* 42 (2006) 156.

[12] J. Lantz, R. Grdhagen and M. Karlsson, "Quantifying turbulent wall shear stress in a subject specific human aorta using large eddy simulation," *Med Eng Phys.*2012 Oct 34(8):1139-48.

[13] C. Cheng, D. Tempel, R. Van Haperen, D. M. Van Der Baan, F. Grosveld and M. J. Daemen et al,"Atherosclerotic lesion size and vulnerability are determined by patterns of fluid shear stress," *CIRCULATIONAHA* 113(June):2744-53.

[14] A. Frydrychowicz, A. F. Stalder, M. F. Russe, J. Bock, S. Bauer and A. Harloff et al. "Three-dimensional analysis of segmental wall shear stress in the aorta byflow-sensitive four-dimensional-MRI," *J Magn Reson Imaging 2009* 30(July):77-84.

[15] C. Irace, C. Cortese, E. Fiaschi, C. Carallo, E. Farinaro and A. Gnasso, "Wall shear stress is associated with intima-media thickness and carotid atherosclerosis in subjects at low coronary heart disease risk," *Stroke 2004;* 2009;35(February):464-468.

[16] F. Gao and T. Matsuzawa, "FSI within Aortic Arch Model over Cardiac Cycle and Influence of Wall Stiffness on Wall Stress in Layered Wall," *Engineering Letters* 13:2,EL 13 2 15.

[17] F. Ene, "Fluid structure interaction in abdominal aortic aneurysm using ANSYS Workbench", *GMEDTECH.*

[18] M. Loeys, F.M. Van Oosterhout, Q.C.M. Barge Schaapveld, Luc Cozijnsen, L. Braam, A. Waalewijn, A.A.M. Schepens and L. Bart, "Practical Advice for the Cardiologist What Is New in Dilatation of the Ascending Aorta? : Review of Current Literature and Practical Advice for the Cardiologist," *CIRCULATIONAHA.110.949131* Circulation. 2011; 123:924-928.

[19] M. Mnsch and M. Breuer, "Numerical simulation of fluid-structure interaction using eddy-resolving schemes," *Lecture Notes in Computational Science and Engineering* pp. 221-254, Springer, Berlin, Germany, 2010.

[20] B. Friedrich-Karl, D. Hans, J. Pei, S. Schuster, and B. Wan, "A Comparison of One-Way and Two-Way Coupling Methods for Numerical Analysis of Fluid-Structure Interactions," *Journal of Applied Mathematics* Volume 2011 (2011), Article ID 853560.

[21] R.M. Nerem, "Vascular Fluid Mechanics, the Arterial Wall, and Atherosclerosis," *J. Biomech. Eng.* 114, 1992, pp. 274 - 282.

[22] J. M. Hyman, R. Knapp,and J. C. Scovel, "High Order Finite Volume Approximations of Differential Operators on Nonuniform Grids," *Physica D: Nonlinear Phenomena* Volume 60, Issues 14, 1 November 1992, Pages 112-138.

[23] P. E. Vincent, A. M. Plata, A. A. E. Hunt, P. D. Weinberg and S. J. Sherwin, "Blood flow in the rabbit aortic arch and descending thoracic aorta," *J. R. Soc. Interface* (2011) 8, 1708 -1719.

[24] K. Prektold, M. Prosi, "Computational models of arterial flow and mass transport," *Cardiovascular Fluid Mechanics,Springer, Berlin* 2003, pp. 73-134.

[25] T.J. Pedley, "Arterial and venous fluid dynamics, in: G. Pedrizetti, K. Prektold (Eds.), " *Cardiovascular Fluid Mechanics, Springer, Berlin* 2003, pp. 1-72.

[26] N. Shahcheragi, H.A. Dwyer, A.Y. Cheer, A.I. Barakat and T. Rutaganira, "Unsteady and three-dimensional simulation of blood flow in the human aortic arch," *ASME J. Fluids Eng.* 124 (2002) 378-387.

[27] Y. Tokuda, M. H. Song, Y. Ueda, A. Usui, T. Akita, S. Yoneyama and S. Maruyama, "Three-dimensional numerical simulation of blood flow in the aortic arch during cardiopulmonary bypass," *Eur. J. Cardiothorac. Surg.* 33 (2008) 164 167.

[28] T.J. Pedley, "Patrick Nataf and Emmanuel Lansac, Dilation of the thoracic aorta: medical and surgical management," *Heart. 2006 September*92(9): 1345 1352.

[29] E. Claes, J.M. Atienza, G.V. Guinea, F.J. Rojo, J.M. Bernal, J.M. Revuelta and M. Elices, "Mechanical Properties of Human Coronary Arteries," *MADR.IB-CM/S-SAL/0312/2006*.

[30] M. Nakamura, S. Wada, T. Yamaguchi "Computational Analysis of Blood Flow in an Integrated Model of the Left Ventricle and the Aorta," *Journal of Biomechanical Engineering*.

[31] T.J. Pedley, "Arterial and venous fluid dynamics, in: G. Pedrizetti, K. Prektold (Eds.)," *Cardiovascular Fluid Mechanics, Springer, Berlin* 2003, pp. 1-72.

[32] C. Lawrence, "Heart Disease: An Essential Guide for the Newly Diagnosed," *Philadelphia, PA: Perseus Books Group*.

[33] A. Silverstein et. al,"Heart Disease: Twenty-First Century Medical Library," *Breckenridge, CO: Twenty-First Century Books*.

[34] L. Altman, "More Orgasm, More Years of Life?" *NewYorkTimes.com* February 24, 2010.

[35] Z. Keshavarz-Motamed, "Flow Dynamics in Human Aorta with Coexisting Models of Bicuspid Aortic Stenosis and Coarctation of the Aorta," *Doctoral thesis dissertation* Concordia University, 2011.

[36] D. Gallo, G. De Santis, F. Negri, D. Tresoldi, R. Ponzini, D. Massai, M.A. Deriu, P. Segers, B. Verhegghe and G. Rizzo, "On the Use of In Vivo Measured Flow Rates as Boundary Conditions for Image-Based Hemodynamic Models of the Human Aorta: Implications for Indicators of Abnormal Flow," *Ann Biomed Eng.*2012 Mar;40(3):729-41.